

## RESEARCH ARTICLE

10.1002/2016JB013125

## Key Points:

- Predicted diurnal and semidiurnal polar motion variations are evaluated using GPS observations
- Closure between observations and predictions is less than 10 microarcseconds
- Closure improves when simultaneously accounting for libration and ocean tide effects

## Supporting Information:

- Supporting Information S1
- Data Set S1

## Correspondence to:

S. D. Desai,  
shailen.desai@jpl.nasa.gov

## Citation:

Desai, S. D., and A. E. Sibois (2016), Evaluating predicted diurnal and semidiurnal tidal variations in polar motion with GPS-based observations, *J. Geophys. Res. Solid Earth*, 121, 5237–5256, doi:10.1002/2016JB013125.

Received 25 APR 2016

Accepted 9 JUN 2016

Accepted article online 12 JUN 2016

Published online 8 JUL 2016

## Evaluating predicted diurnal and semidiurnal tidal variations in polar motion with GPS-based observations

Shailen D. Desai<sup>1</sup> and Aurore E. Sibois<sup>1</sup>
<sup>1</sup>Jet Propulsion Laboratory, California Institute of Technology, Pasadena, California, USA

**Abstract** We evaluate models for the predicted diurnal and semidiurnal tidal variations in polar motion using observations based upon the Global Positioning System (GPS). The GPS-based observations are composed of 10 year continuous time series of polar motion estimates with 15 min temporal resolution. Predicted effects account for the contributions from ocean tide angular momentum and libration. We consider two models for the predicted ocean tide effects, both of which have their heritage with the so-called TPXO hydrodynamic models of the ocean tide heights and currents that assimilate satellite altimetry, for example, Egbert et al. (1994) and Egbert and Erofeeva (2002). When considering libration effects we use the model from Mathews and Bretagnon (2003). Of the models considered in this study, the best consistency with the GPS-based observations is achieved with predictions from the most recent (version 8) TPXO-based model for ocean tide effects together with the model for libration effects. This combination demonstrates closure of the budget between predicted and GPS-based observations at the level of less than 10, 2, and 5  $\mu$ as in prograde diurnal, prograde semidiurnal, and retrograde semidiurnal tidal variations in polar motion, respectively. The observations also demonstrate inconsistency between the older TPXO-based model for ocean tide effects and the libration model, both of which are currently recommended by the International Earth Rotation Service.

## 1. Introduction

Through the conservation of angular momentum, mass redistribution within the Earth system and the application of external torques to that system cause variations in the rotation of the solid Earth [e.g., *Munk and Macdonald*, 1960]. These variations are typically decomposed into the axial and non-axial components of the Earth's rotation vector, namely, the Earth's rotation rate and the orientation of the rotation axis, respectively. The variations in the orientation of the rotation axis are typically segregated into polar motion and nutation components given that observations of the rotation axis are dependent on the viewing reference frame. Variations with frequency  $\omega$  as observed in the terrestrial reference frame appear as variations with frequency  $\omega + \Omega$  when observed in the celestial reference frame [e.g., *Gross*, 2015], where  $\Omega$  is the mean rotation rate of the Earth of 1 cycle per sidereal day (cpsd). By convention [e.g., *Petit and Luzum*, 2010], nutation is considered to represent variations of the Earth's rotation axis with frequencies between  $-1.5$  and  $-0.5$  cpsd as viewed in the terrestrial reference frame or alternatively frequencies within  $\pm 0.5$  cpsd as viewed in the celestial frame (see, for example, a historical discussion by *Gross* [2015]). Positive and negative frequencies indicate prograde and retrograde variations of the rotation axis, respectively. In effect, nutation is considered to be limited to the long-period variations of the rotation axis as viewed from the celestial reference frame, while polar motion represents variations at all other periods. Hereinafter, we refer to frequencies in the terrestrial reference frame since the polar motion observations that we use are inherently in this frame.

In this paper, our objective is to evaluate predicted diurnal and semidiurnal tidal variations in polar motion with observations from the Global Positioning System (GPS) space geodetic technique. Diurnal and semidiurnal tidal variations in polar motion are predominantly caused by the ocean tides and have amplitudes of a few hundred microarcseconds ( $\mu$ as) [e.g., *Chao et al.*, 1996]. Specifically, the redistribution of mass from the ocean tide heights causes variations in the Earth's inertia tensor, while the associated tidal currents cause variations in the relative angular momentum of the oceans with respect to the solid Earth. These are referred to as the mass and motion components of the ocean tide effects, respectively. The diurnal ocean tides certainly contribute to retrograde diurnal variations of the Earth's rotation axis. However, we follow conventions by considering them as contributing to observed nutation and do not evaluate them in this study. Modern models of nutation [e.g., *Mathews et al.*, 2002] account for the effects of retrograde diurnal variations

from the ocean tides, along with the significantly larger effects from external lunisolar torques acting on the Earth's equatorial bulge and retrograde diurnal variations caused by the solid Earth tides. An additional contribution to prograde diurnal tidal variations in polar motion results from external lunisolar tidal torques acting on the triaxial Earth figure, with amplitudes up to  $16 \mu\text{as}$  [e.g., *Chao et al.*, 1991; *Getino et al.*, 2001; *Brzeziński and Capitaine*, 2002; *Mathews and Bretagnon*, 2003]. We follow *Chao et al.* [1991] by also referring to these as the libration effects on polar motion. Atmospheric pressure and wind also contribute to diurnal and semidiurnal polar motion but are not considered in this study. While these effects are considered as non-tidal in origin they have non-negligible contributions to polar motion at the  $S_1$  and  $S_2$  (once and twice per solar day, respectively) tidal frequencies and are estimated to have amplitudes of less than  $10 \mu\text{as}$  [Brzeziński et al., 2004]. These atmospheric effects also cause non-gravitational contributions to the ocean tides, again primarily in the  $S_1$  and  $S_2$  frequencies [e.g., *Ray and Egbert*, 2004]. Our approach likely accounts for the non-gravitational contribution to  $S_2$  ocean tide angular momentum but not  $S_1$ , because we use the explicitly provided model of  $S_2$  that is constrained by altimeter observations while inferring  $S_1$  from other tidal frequencies (see Appendix A). We use the GPS-based observations to evaluate the performance of the current, but at least decade-old, conventional model for predicted ocean tide effects [Petit and Luzum, 2010] against a more recent model, as well as their respective compatibility with the model for libration effects.

Models of the ocean tide heights and currents are needed to predict their effects on variations of the Earth's rotation [Gross, 1993]. These effects were originally predicted from theoretical ocean tide models [e.g., *Brosche et al.*, 1989; *Seiler*, 1991]. However, significant advances in predicting these effects have been achieved by using ocean tide models that incorporate almost global sea surface height observations from satellite altimetry [e.g., *Chao et al.*, 1996]. The satellite altimeter data are particularly useful for mapping the ocean tide heights, which are needed to predict the mass component of tidal variations in Earth rotation. The motion component, however, requires knowledge of the tidal currents and ocean depths. Simplified Laplace equations of motion were initially applied to determine the required tidal currents from the global altimeter-based tide height maps [e.g., *Ray et al.*, 1994; *Chao et al.*, 1996]. Subsequently, hydrodynamic ocean tide models constrained by, or assimilating, the altimeter observations were also used, since they explicitly solve for tidal currents (and tide heights) through the rigorous application of equations of motion over the oceans. These hydrodynamic models have an additional benefit in that they provide a dynamic approach for essentially extrapolating the tide heights and currents to the polar latitudes that may not be sampled by the altimeters. They also benefit from assimilating tide gauge observations in these, and other, regions. The current International Earth Rotation Service (IERS) conventions for the predicted effects of the diurnal and semidiurnal ocean tides on polar motion and rotation rate [Petit and Luzum, 2010] (hereinafter referred to as the IERS 2010 model) are derived from the altimetry-dependent hydrodynamic model of *Egbert et al.* [1994], referred to as Model C in *Chao et al.* [1996]. That same model from *Chao et al.* [1996] was also used by *Mathews et al.* [2002] to account for the ocean tide contribution to nutation. Here we derive the predicted effects of the diurnal and semidiurnal ocean tides on polar motion using the TPX08 altimeter-dependent model. This model is a more recent version of the model described by *Egbert and Erofeeva* [2002] as well as Model C that was used by *Chao et al.* [1996]. The TPX08 model effectively incorporates longer durations of the altimeter observations and has higher spatial resolution than its predecessors. It also assimilates tide gauge observations, perhaps most importantly including those in polar regions not sampled by the altimeters, to improve global performance.

Predictions of the libration effects are determined through the application of the lunisolar tidal potential to models of the Earth. Gravity field models are used to provide the required measure of the two equatorial components of the Earth's moment of inertia, through the degree 2 and order 2 Stokes coefficients ( $C_{22}$  and  $S_{22}$ ) of the gravity field. A report from the International Astronomical Union working group on nutation [Brzeziński and Mathews, 2003] identifies *Kinoshita* [1977] as first considering libration effects for a rigid Earth and *Chao et al.* [1991] as providing a first estimate for a non-rigid Earth. These were followed by computations with more rigorous Earth models a decade later [e.g., *Getino et al.*, 2001; *Brzeziński and Capitaine*, 2002; *Mathews and Bretagnon*, 2003]. The libration model from *Mathews and Bretagnon* [2003], with a cutoff of  $0.5 \mu\text{as}$  for included tidal frequencies, has been adopted by the current IERS conventions [Petit and Luzum, 2010]. The effects of the triaxial core of the Earth on libration are intentionally excluded from the conventional model due to a lack of consensus between independent models but are estimated to be no larger than  $2.5 \mu\text{as}$  [Brzeziński and Mathews, 2003].

Data from the space geodetic techniques provide observations of the diurnal and semidiurnal tidal variations in polar motion. Historically, observations have been most extensively determined using the very long baseline interferometry (VLBI) technique [e.g., *Herring and Dong*, 1994; *Gipson*, 1996; *Artz et al.*, 2011]. This technique is faced with the challenge of a relatively small network and gaps between intensive observation campaigns but benefits from a lengthy historical data record. Diurnal and semidiurnal tidal variations in polar motion observed by satellite laser ranging tracking have also been determined [*Watkins and Eanes*, 1994], but this technique is faced with the challenge of sparse and non-uniform data. Global networks of terrestrial GPS stations are also being increasingly used to generate observations of diurnal and semidiurnal tidal variations in polar motion [e.g., *Rothacher et al.*, 2001; *Sibois*, 2011]. The GPS approach has the benefit of continuously available data and a global network that has been growing since the early 1990s. However, the GPS approach is prone to systematic errors most significantly from mismodeling of solar radiation pressure forces acting on the satellites and therefore potentially at solar tidal frequencies. Recently, *Artz et al.* [2012] have used a combination of VLBI and GPS data but they concede that their diurnal and semidiurnal tidal polar motion estimates are dominated by the GPS data.

Our approach for evaluating predicted with observed diurnal and semidiurnal tidal variations in polar motion is to apply background models for the predicted tidal effects when generating GPS-based polar motion observations. We then generate continuous time series of residual polar motion with 15 min temporal resolution using data from global networks of GPS tracking stations. These observations of residual polar motion reflect remaining unmodeled effects (e.g., atmospheric effects in this case) and errors in the background models. We use observed residual signals at tidal frequencies as a measure of deficiencies in the background models. This contrasts to the alternative approach that explicitly compares predicted and observed tidal amplitudes and phases or alternatively in-phase and quadrature terms [e.g., *Artz et al.*, 2011; *Englich et al.*, 2007]. In the latter approach, observations of the tidal components are determined either directly through inclusion into the normal equations associated with the geodetic data or indirectly from high-frequency (e.g., sub-hourly, hourly, or 2 h) time series of observed polar motion that have been generated without the application of background models.

We compare the performance of two models of predicted diurnal and semidiurnal ocean tide contributions to polar motion. The first is the IERS 2010 model that has been recommended for over a decade. The second is based upon our computations of predicted effects as derived from the more recent TPX08 ocean tide model. Since TPX08 is a more recent version of the ocean tide model used to derive the IERS 2010 model for ocean tide effects on Earth rotation (Model C from *Chao et al.* [1996]), results from this study provide an additional external metric to evaluate enhancements to these models. We consider each model of ocean tide effects with and without application of the predicted diurnal libration effects using the IERS conventional model from *Mathews and Bretagnon* [2003]. Of interest is the consistency of the sum total of the predicted ocean tide and libration effects with observed prograde diurnal polar motion, since the predictions of each effect are completely independent of each other. The best consistency should result in the lowest observed residual diurnal tidal signal. Note that *Chao et al.* [1996] found that the respective accuracies of the predicted ocean tide effects and VLBI-based observations available at that time were insufficient to evaluate their model of the libration effects. Other studies [e.g., *Artz et al.*, 2012] have found incompatibilities between their observations and the IERS 2010 models for predicted ocean tide and libration effects. Consistent with our previously stated approach to exclude evaluation of nutation in this study, we always apply the background nutation model from *Mathews et al.* [2002], as recommended by the current IERS conventions [*Petit and Luzum*, 2010], when generating the GPS-based polar motion time series. In effect, this means that we always use Model C from *Chao et al.* [1996], in the manner in which it has been applied to that nutation model, to account for the ocean tide effects on retrograde diurnal motion of the rotation axis.

## 2. Predicted Ocean Tide Effects on Polar Motion

The geodetic techniques report polar motion as the location of the rotation axis in the direction of the Greenwich and 90°W meridians,  $p_1$  and  $p_2$  (or  $x$  and  $y$  directions), respectively. These are related to the prograde ( $p$ ) and retrograde ( $r$ ) components as follows, with respective amplitudes and phases,  $A_p$ ,  $A_r$ ,  $\alpha_p$ , and  $\alpha_r$  [e.g., *Chao et al.*, 1996].

$$p(t) = p_1(t) - ip_2(t) = A_p e^{i(\theta(t) + \alpha_p)} + A_r e^{-i(\theta(t) - \alpha_r)}. \quad (1)$$

**Table 1.** Mass and Motion Components of Ocean Tide Angular Momentum,  $\Omega c_{i3}$  and  $h_i$  ( $i = 1, 2, 3$  for  $x$ ,  $y$ , and  $z$ ), Respectively, for the Eight Primary Diurnal and Semidiurnal Tidal Components From the TPX08 Ocean Tide Model<sup>a</sup>

	Q <sub>1</sub>		O <sub>1</sub>		P <sub>1</sub>		K <sub>1</sub>		N <sub>2</sub>		M <sub>2</sub>		S <sub>2</sub>		K <sub>2</sub>	
	A	$\phi$	A	$\phi$	A	$\phi$	A	$\phi$	A	$\phi$	A	$\phi$	A	$\phi$	A	$\phi$
<i>X</i>																
Mass	1.2	341	4.7	330	1.5	315	4.6	309	1.3	349	5.1	10	1.2	41	0.3	40
Motion	0.6	322	2.6	311	1.4	291	4.9	289	1.3	253	10.2	260	5.8	300	1.7	294
<i>Y</i>																
Mass	2.6	216	11.8	222	4.4	224	13.9	224	0.3	240	3.5	305	2.9	8	0.8	7
Motion	0.6	228	4.0	214	2.0	197	7.1	196	2.5	164	17.9	168	9.8	203	2.8	197
<i>Z</i>																
Mass	0.7	141	1.9	169	0.4	19	1.6	9	0.5	69	6.0	84	2.5	126	0.7	124
Motion	1.4	109	6.2	119	2.4	128	7.8	129	3.0	330	15.8	319	7.8	344	2.2	343

<sup>a</sup>Amplitudes,  $A$ , and Greenwich phase lags,  $\phi$ , have units of  $10^{24} \text{ kg m}^2 \text{ s}^{-1}$  and degrees, respectively.

The astronomical tidal argument,  $\theta(t) = \omega t + \beta$ , is a function of the tidal frequency,  $\omega$ , and associated phase,  $\beta$ . We compute the predicted effects of the ocean tides on polar motion following the approach adopted by Gross [1993] and Chao *et al.* [1996]. Specifically, we use equation 4.18 of Sasao and Wahr [1981] provided in the frequency domain, given the relationship between nutation and reported polar motion from Gross [1992]. This computation of the predicted ocean tide effects on polar motion is repeated here for clarity.

$$\mathbf{p}(\omega) = \left[ 2.554 \times 10^{-4} \frac{\Omega}{\omega_{fcn} - \omega} + 2.686 \times 10^{-3} \frac{\Omega}{\omega_{cw} - \omega} \right] \frac{\Omega \mathbf{c}(\omega)}{A \Omega \tau} + \left[ 6.170 \times 10^{-4} \frac{\Omega}{\omega_{fcn} - \omega} + 1.124 \frac{\Omega}{\omega_{cw} - \omega} \right] \frac{\mathbf{h}(\omega)}{A \Omega} \quad (2)$$

In this equation  $\omega_{fcn}$  is the frequency of the Earth's free core nutation ( $-1-1/431.4$  cpsd) [Mathews *et al.*, 2002],  $\omega_{cw}$  is the frequency of the Chandler wobble ( $1/434.3$  cpsd with  $Q = 170$ ) [Wilson and Vicente, 1980],  $\Omega = 1$  cpsd,  $\tau = \Omega^2 a^5 / 3GA$ ,  $a$  is the mean radius of the Earth,  $G$  is the universal gravitational constant, and  $A$  is the Earth's mean equatorial moment of inertia. The complex quantities  $\mathbf{c}(t) = c_{13}(t) + ic_{23}(t)$  and  $\mathbf{h}(t) = h_1(t) + ih_2(t)$  represent the equatorial ( $x$  and  $y$ ) mass and motion components of the ocean tide contributions to polar motion, respectively. The former represents perturbations to the indicated components of the Earth's inertia tensor from the redistribution of mass associated with the ocean tide heights. The latter represents the perturbations to oceanic angular momentum relative to the solid Earth from the ocean tide currents. Similarly, variations in the Earth's rotation rate, or length-of-day (LOD), are dependent on perturbations to the polar moment of inertia,  $c_{33}(t)$ , and axial ( $z$ ) component of relative angular momentum,  $h_3(t)$  [e.g., see Gross, 1993, equation (6)]. Formulas for computing each of these quantities are provided, for example, in equations (1) and (2) from Chao and Ray [1997]. The angular momentum functions are actually functions of mass transport, namely, the product of ocean depth and tidal ocean current velocities. Here we also use a value of  $1035 \text{ kg/m}^3$  for the density of sea water.

We use version 8 of the TPX0 model, TPX08, for the eight primary diurnal and semidiurnal ocean tides to compute the respective mass and motion contributions to angular momentum, as shown in Table 1. This is a more recent version of the hydrodynamic model from Egbert *et al.* [1994] and Egbert and Erofeeva [2002] that assimilates satellite altimeter measurements of tide heights. The model provides global maps of tide heights and two-dimensional (east-west and north-south) mass transport. The model is distributed with 2 min global spatial resolution in latitude and longitude. The released tidal fields are based upon a 1/6th-degree global data assimilative model merged with 33 higher resolution (1/30th-degree) regional solutions (G. Egbert, personal communication, 2016). The model's provision of mass transport, rather than tidal currents, is convenient for predicting variations in the Earth orientation parameters (EOPs), which include polar motion and LOD. The predicted mass transport perhaps has some benefit in having improved consistency with the accurate tide height measurements provided by the satellite altimeter measurements. Only the equatorial,  $x$  and  $y$ , components of angular momentum are required for predicting the effects of the ocean tides on polar motion and nutation. However, for completeness and consistency, Table 1 also provides the axial,  $z$ , component as it can be applied toward predicting tidal variations in LOD.

The ocean tide angular momentum budgets of *Chao et al.* [1996] have essentially served as a reference for the last two decades by virtue of their application to the IERS 2010 model for predicting tidal variations in the EOPs, as well as their use in the conventional nutation model from *Mathews et al.* [2002]. For ease of comparison, in Table 1 we intentionally adopt the Greenwich phase lag convention that is typically adopted by most ocean tide models and that was used in Table 3 of *Chao et al.* [1996]. Recall that their values are based upon one of the early versions of the TPXO ocean tide model. Vector differences between the TPXO8-based values with those from *Chao et al.* [1996] are generally larger for the motion than the mass component. For example, only the  $y$  component of the  $M_2$  and  $K_1$  tides have mass component differences larger than  $0.5 \cdot 10^{24} \text{ kg m}^2 \text{ s}^{-1}$ . However, two axial ( $z$ ) and seven equatorial ( $x$  and  $y$ ) motion terms have differences that are larger than  $0.5 \cdot 10^{24} \text{ kg m}^2 \text{ s}^{-1}$ , with the  $K_1$   $y$  component having the largest difference of  $1.3 \cdot 10^{24} \text{ kg m}^2 \text{ s}^{-1}$ . This suggests that the most significant evolution in the TPXO tide modeling approach has been with the determination of mass transport. This is perhaps as expected given that the long-wavelength components of the ocean tide heights needed to predict the mass component have been well determined from the altimeter observations. Although, advances in modeling the ocean tides at the polar latitudes not sampled by the altimeters [e.g., *Ray et al.*, 1996] are also important for accurate determination of these long-wavelength components.

To determine the significance of these differences in the ocean tide angular momentum budget we apply them toward predicting their impact on the EOPs. However, explicit ocean tide models are not provided for all tidal frequencies in the diurnal and semidiurnal tidal spectrum. In the diurnal and semidiurnal tidal bands they are usually provided for at least the eight primary components shown in Table 1. The typical approach is to then infer the ocean tide response, and consequently their predicted effects on the EOPs, at other tidal frequencies by assuming a smooth unit relative response within each tidal band, or within narrow bands close to those primary frequencies. Appendix A provides details on the response function approach that we used to compute the TPXO8-based predicted effects of the ocean tides on the EOPs at all diurnal and semidiurnal tidal frequencies. We determine smooth response functions for each of the EOPs and in each of the diurnal and semidiurnal bands using the respective predicted variations at the primary frequencies explicitly provided by the TPXO8 model. Appendix A also provides tables of the respective predicted diurnal and semidiurnal variations in polar motion and LOD at 159 tidal frequencies. Although our primary objective is to evaluate polar motion, we also compute and provide predicted LOD variations. For complete consistency we simultaneously apply background models of the TPXO8-based predicted tidal variations in polar motion and LOD when generating the respective GPS-based observations of residual polar motion. Similarly, when generating GPS-based observations of residual polar motion with the IERS 2010 background model we use values of predicted tidal variations in polar motion and LOD as provided in Tables 8.2a, 8.2b, 8.3a, and 8.3b of *Petit and Luzum* [2010]. These IERS 2010 values at 71 tidal frequencies were determined by applying a smooth response approach to the *Chao et al.* [1996] Model C predicted EOP variations at the eight primary frequencies.

Our approach for evaluating differences between polar motion predictions from different ocean tide models can be considered as follows. Each individual model for the  $x$  and  $y$  polar motion variations,  $p_1$  and  $p_2$ , respectively, can be considered to have coefficients  $C_x$ ,  $S_x$ ,  $C_y$ , and  $S_y$  for the in-phase (cosine) and quadrature (sine) components of the tidal argument  $\theta(t)$  (see equation (1)). Respective differences between models, or model errors, are represented by  $\delta C_x$ ,  $\delta S_x$ ,  $\delta C_y$ , and  $\delta S_y$ . From equation (1), each of the prograde and retrograde polar motion vectors is then as follows.

$$A_p \cos \alpha_p + i A_p \sin \alpha_p = \frac{1}{2} [(C_x + \delta C_x) - (S_y + \delta S_y)] - i [(S_x + \delta S_x) + (C_y + \delta C_y)]. \quad (3a)$$

$$A_r \cos \alpha_r + i A_r \sin \alpha_r = \frac{1}{2} [(C_x + \delta C_x) + (S_y + \delta S_y)] + i [(S_x + \delta S_x) - (C_y + \delta C_y)]. \quad (3b)$$

Subsequently, we use the amplitudes of the differences in each of the prograde and retrograde polar motion vectors to evaluate model discrepancies.

$$\text{Prograde : } \Delta_p = \frac{1}{2} \sqrt{(\delta C_x - \delta S_y)^2 + (\delta S_x + \delta C_y)^2}. \quad (4a)$$

$$\text{Retrograde : } \Delta_r = \frac{1}{2} \sqrt{(\delta C_x + \delta S_y)^2 + (\delta S_x - \delta C_y)^2}. \quad (4b)$$

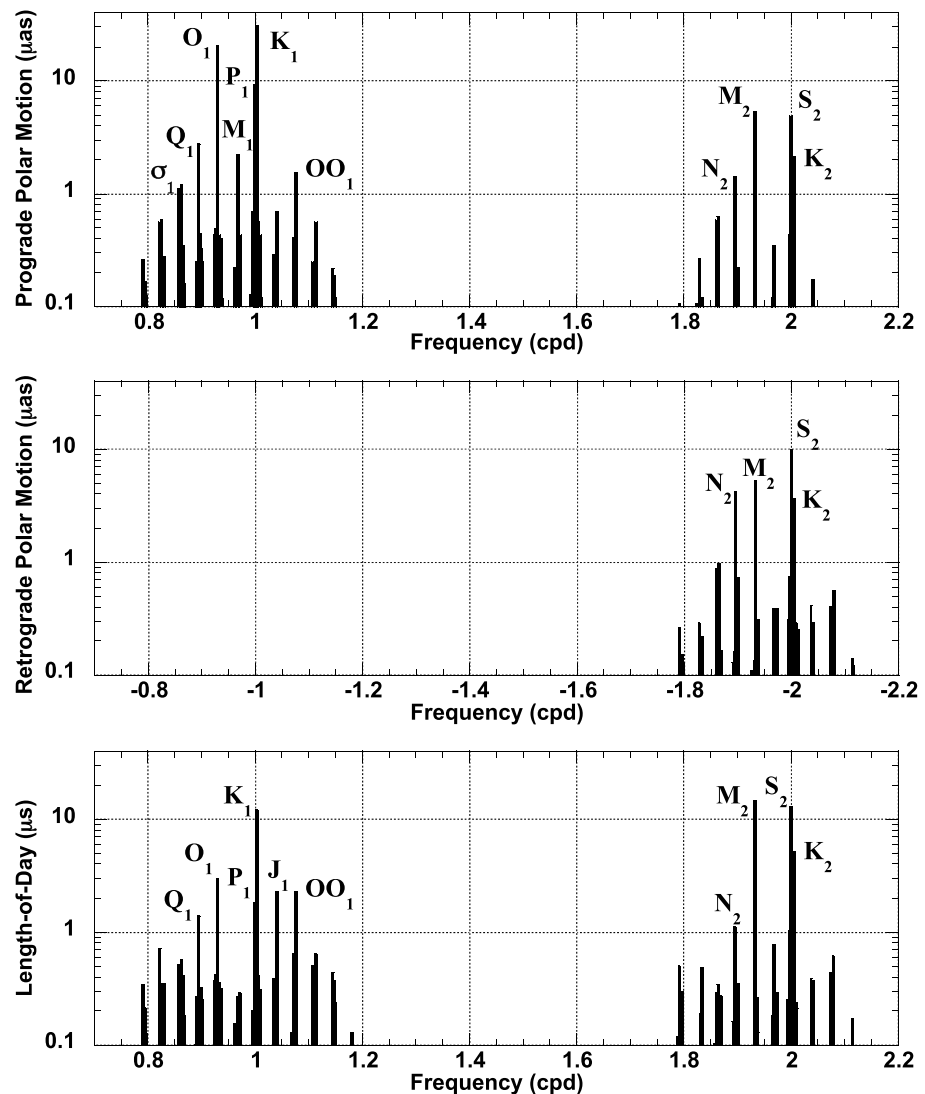


**Figure 1.** Amplitude of differences between this paper's and the IERS 2010 models for predicted diurnal and semidiurnal ocean tide effects on variations in polar motion and length-of-day. This paper's values are based upon the TPX08 ocean tide model, while the IERS 2010 model is based upon Model C (an earlier TPX0 model) from *Chao et al. [1996]*. Differences are shown for (top) prograde polar motion, (middle) retrograde polar motion, and (bottom) length-of-day. The root-sum-square of these differences are  $39.5 \mu\text{s}$ ,  $13.0 \mu\text{s}$ , and  $24.8 \mu\text{s}$ , respectively. Both models being differenced have no diurnal retrograde components by convention.

As expected, the most significant differences between the TPX08-based values and those from the IERS 2010 model are in the eight primary diurnal and semidiurnal tidal components, as is evident from Figure 1. Polar motion differences are largest in the diurnal band with amplitudes of  $2.8$ ,  $20.4$ ,  $9.4$ , and  $30.5 \mu\text{s}$  for the  $Q_1$ ,  $O_1$ ,  $P_1$ , and  $K_1$  retrograde components, respectively. In the semidiurnal band, differences in the prograde (retrograde) components are  $1.4$  ( $4.2$ ),  $5.4$  ( $5.3$ ),  $4.9$  ( $10.1$ ), and  $2.1$  ( $3.7$ )  $\mu\text{s}$  for the  $N_2$ ,  $M_2$ ,  $S_2$ , and  $K_2$  components, respectively. Length-of-day differences are largest for the  $O_1$ ,  $K_1$ ,  $M_2$ ,  $S_2$ , and  $K_2$  components with amplitudes of  $3.0$ ,  $12.2$ ,  $14.8$ ,  $13.2$ , and  $5.2$  microseconds ( $\mu\text{s}$ ), respectively. Most importantly, these differences are at the same level as, or larger than, the total effects of libration on diurnal polar motion and semidiurnal LOD. They are therefore significant with regard to closing the budget between observed and predicted tidal variations in the EOPs.

### 3. Evaluation Using GPS-Based Polar Motion Observations

We use GPS-based observations to evaluate models for the predicted effects of the ocean tides and libration on diurnal and semidiurnal polar motion. Our approach applies background models for the predicted effects

when generating GPS-based time series of observed residual polar motion. For each considered background model, or combination of models, continuous GPS-based observations of residual polar motion are generated with 15 min temporal resolution spanning 10 years, 2004–2013. In cases where a background model for the effects of libration on polar motion and rotation rate is applied we use the conventional model from *Mathews and Bretagnon* [2003], as provided in Tables 5.1a and 5.1b in *Petit and Luzum* [2010]. In all cases, daily values of polar motion and Earth rotation rate from the IERS EOPC04 time series are also applied as background nominal values when processing the GPS data. In effect, these daily values serve to model variations in the EOPs at periods longer than 2 days. However, they also contain daily averages of errors in the background models of diurnal and semidiurnal EOP variations that were applied when generating those values. The IERS 2010 model is likely to have been used by most of the contributors to these daily time series given that it has been the recommended model for over a decade. Also, in all cases the conventional nutation model from *Mathews et al.* [2002] is applied, serving to model diurnal retrograde motion of the rotation axis caused by the ocean tides and other effects, as mentioned earlier.

The GPS processing approach essentially follows that described in *Sibois* [2011]. Independent GPS network solutions are performed daily using data spanning 3 days, with each solution also estimating GPS satellite and station states, as well as tropospheric delay at each station. A potential benefit from applying background models of polar motion is to mitigate the impact of correlations between other parameters in the GPS network solutions on the estimated residual polar motion parameters of interest to this study [e.g., *Sibois*, 2011]. In each 3 day network solution polar motion is estimated at 15 min intervals using 5 min GPS tracking data from 60 globally distributed terrestrial GPS sites. The positions of approximately 25% of the stations are fixed to the International Global Navigation Satellite Systems (GNSS) Service (IGS) realization of the 2008 International Terrestrial Reference Frame [*Altamimi et al.*, 2011], while the remainder are estimated. The 10 year time series of residual polar motion are then generated by accumulating the middle 24 h of 15 min estimates from each daily 3 day solution. This approach inherently has the risk of introducing daily discontinuities which can manifest as harmonics of the 24 h period. However, these are mitigated through our approach to estimate residual, rather than total, polar motion.

Equations (3) and (4) are similarly applied to evaluating the background models. In this case,  $C_x$ ,  $S_x$ ,  $C_y$ , and  $S_y$  represent the coefficients of the background models. Spectral decompositions of the GPS-based observed residual polar motion time series then provide estimates of  $\delta C_x$ ,  $\delta S_x$ ,  $\delta C_y$ , and  $\delta S_y$ . In this case, these coefficients represent residual errors in the background models, namely, the difference between total observed and background model prograde and retrograde vectors, and systematic errors introduced by the GPS processing approach. The amplitude of the error vector is then provided by equation (4).

The case that applies background models for the sum total of the ocean tide and libration effects on the EOPs using the TPX08-based predictions of the ocean tide effects is chosen as a reference solution. Figure 2 shows that the background noise in the GPS-based time series of residual polar motion is mostly below 2  $\mu\text{as}$  in the prograde diurnal tidal band, and always below 1  $\mu\text{as}$  in the prograde and retrograde semidiurnal tidal bands. The exception is within  $\pm 0.05$  cycles per day (cpd) of the 1 cpd diurnal frequency where background noise and systematic signals reach 5–10  $\mu\text{as}$ . Our approach for accumulating the 10 year time series from the middle 24 h of 3 day solutions as well as expected systematic errors from mismodeling solar radiation pressure forces on the GPS satellites are likely contributors to larger errors near 1 cpd. The largest residual signal is at a frequency of 0.983 cpd (24.4 h) and has an amplitude of 11  $\mu\text{as}$  but does not correspond to any known tidal frequency. Otherwise, residual signals primarily occur at the tidal frequencies and are clearly distinguishable above the background noise. In the prograde diurnal band the residual errors in the background models are always less than 10  $\mu\text{as}$ , and in the prograde semidiurnal band they are all less than 2  $\mu\text{as}$ . With the exception of  $S_2$ , residual errors in the retrograde semidiurnal band are less than 5  $\mu\text{as}$ . Recall that we have not accounted for atmospheric effects that are known to have contributions at the  $S_1$  and  $S_2$  tidal frequencies of less than 10  $\mu\text{as}$  [*Brzeziński et al.*, 2004]. Larger residual signals in the retrograde semidiurnal band than prograde are expected since the total signal is at least 3 times larger. Of note are the residual signals at the  $OO_1$ ,  $2N_2$ , and  $\mu_2$  tidal frequencies which have residual signal with similar amplitudes as the total predicted background models themselves. As described in Appendix A, we expect larger errors for tidal frequencies, such as these, that are outside of the range spanned by the primary frequencies from which the EOPs are derived for the respective tidal bands.

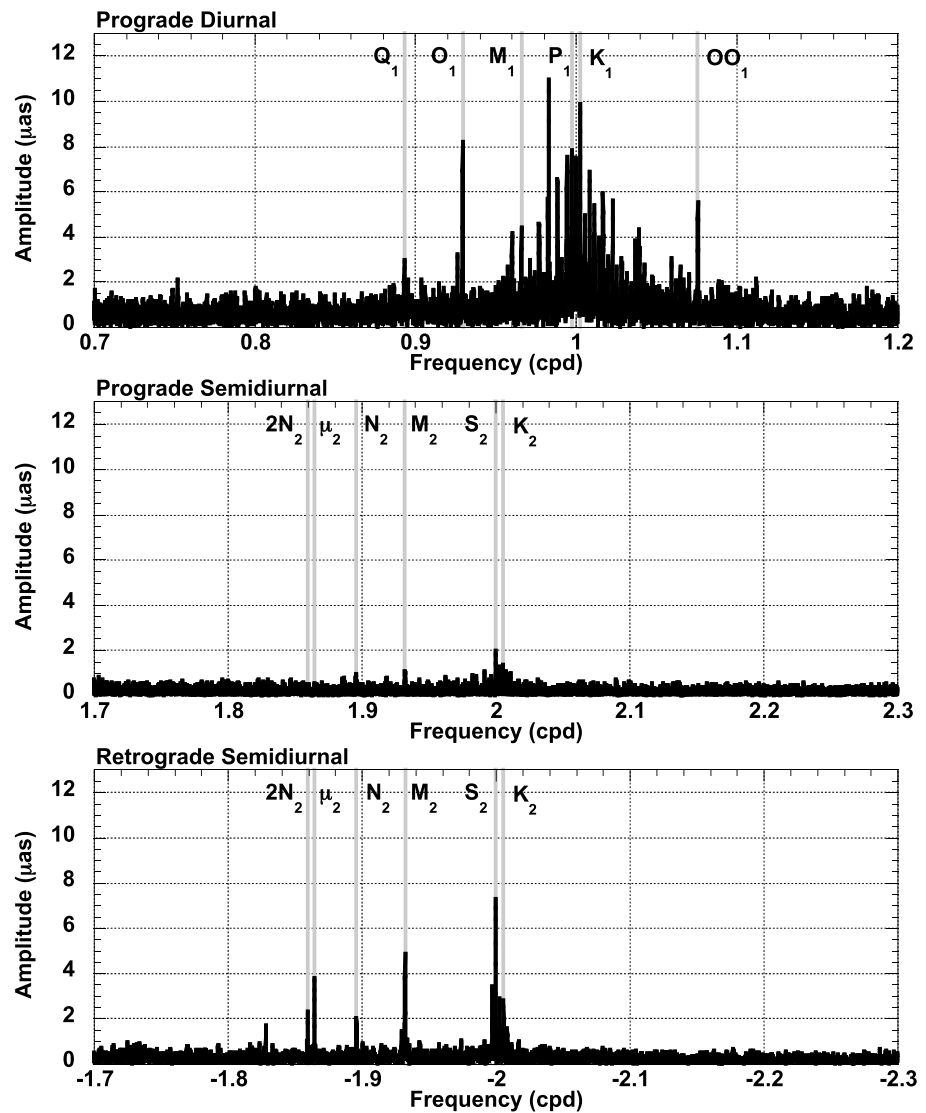


**Figure 2.** Amplitude spectrum of GPS-based observations of residual variations in the (top) prograde diurnal, (middle) prograde semidiurnal, and (bottom) retrograde semidiurnal tidal frequency bands when applying background models for ocean tide effects from this paper's TPX08-based model and libration effects from *Mathews and Bretagnon* [2003]. Gray lines indicate frequencies of some primary tidal components.

As an alternative approach, we also perform a least squares analysis of the reference GPS-based residual polar motion time series, estimating only the tidal signals along with bias, drift, and harmonic signals at periods of 4, 4.8, 6, 8, and 32.9 h. Systematic signals at the level of 1–5  $\mu\text{as}$  are observed at these periods but clearly non-tidal in origin. The error coefficients  $\delta C_x$ ,  $\delta S_x$ ,  $\delta C_y$ , and  $\delta S_y$  are explicitly estimated at 180 narrow tidal bands. A constant relative response of all tidal frequencies within 1 cycle per year of each primary frequency in each of those bands is assumed. The formal (1 sigma) errors of the estimated error coefficients at tidal frequencies are all on the order of 0.1–0.3  $\mu\text{as}$ , except for  $S_1$  at 0.4  $\mu\text{as}$ , suggesting they have accuracies of better than 1.5  $\mu\text{as}$  even if using a conservative 5 sigma estimate of the errors. The resulting prograde and retrograde error vector amplitudes (equations (4a) and (4b)), as shown in Table 2, agree well with the spectral decomposition in Figure 2, especially for the semidiurnal frequencies where the background noise is low. Discrepancies of up to 2  $\mu\text{as}$  are apparent for the prograde diurnal frequencies, especially for frequencies near 1 cpd where the background systematic signals are larger and not explicitly accommodated in the least squares approach. The results in Table 2 reinforce that all residual tidal signals are less than 10  $\mu\text{as}$  when using background models with the TPX08-based ocean tide effects together with the libration effects.

**Table 2.** Amplitudes of Residual Tidal Signals in GPS-Based Observations of Polar Motion When Applying Background Models for Libration Effects From *Mathews and Bretagnon* [2003] and Ocean Tide Effects From the Two Considered Models, This Paper's TPX08 and the IERS 2010 Models<sup>a</sup>

Tide	Direction	Background Ocean Tide Model	
		TPX08	IERS 2010
Q <sub>1</sub>	Prograde	2.8	5.1
O <sub>1</sub>	Prograde	7.4	7.5
M <sub>1</sub>	Prograde	0.7	2.4
$\pi_1$	Prograde	3.0	3.0
P <sub>1</sub>	Prograde	7.8	2.8
S <sub>1</sub>	Prograde	8.8	8.7
K <sub>1</sub>	Prograde	8.0	24.6
$\psi_1$	Prograde	3.5	3.5
J <sub>1</sub>	Prograde	3.7	2.7
OO <sub>1</sub>	Prograde	4.1	3.1
M <sub>2</sub>	Prograde	0.9	5.7
S <sub>2</sub>	Prograde	2.1	4.1
2 N <sub>2</sub>	Retrograde	2.5	1.6
$\mu_2$	Retrograde	3.9	3.1
N <sub>2</sub>	Retrograde	2.0	3.7
M <sub>2</sub>	Retrograde	5.0	7.4
T <sub>2</sub>	Retrograde	3.3	2.8
S <sub>2</sub>	Retrograde	7.4	7.2
K <sub>2</sub>	Retrograde	0.9	4.3

<sup>a</sup>Retrograde diurnal signals are not considered, and only those tidal frequencies with residual signals larger than 2  $\mu$ as for either model are shown. Results are based upon least squares analysis of residual GPS-based time series of polar motion. Units are  $\mu$ as.

Also shown in Table 2 are the corresponding results when using the IERS 2010 model for ocean tide effects together with the libration model. The comparison with the respective TPX08-based case is visualized in Figures 3 (top panel) and 4. Most notable is the significant improvement in performance, as manifested by smaller amplitudes of residual signals, when using the TPX08-based model at most of the primary tidal frequencies. In particular, the residual tidal errors in the prograde Q<sub>1</sub>, K<sub>1</sub>, and M<sub>2</sub> variations and the retrograde N<sub>2</sub>, M<sub>2</sub>, and K<sub>2</sub> variations are smaller by 2–16  $\mu$ as when using the TPX08-based model. When the TPX08-based model generates larger residual errors than the IERS 2010 model the increase is always less than 1  $\mu$ as with one exception. Overall, these results suggest that the TPX08-based model provides minimal impact on the minor tidal components compared to the IERS 2010 model. In the one exception, the amplitude of the residual error in the prograde P<sub>1</sub> component increases by 5  $\mu$ as when using the TPX08-based model.

The least squares approach used to generate Table 2 indicates that the TPX08 and IERS 2010 models result in similar (within 0.1  $\mu$ as) residual variations at the prograde O<sub>1</sub> tidal component. Similarly, in the spectral approach used to generate Figure 3 the closest reported frequency to the O<sub>1</sub> component shows residual variations from the TPX08 and IERS 2010 models agreeing to within 0.2  $\mu$ as, while the other (further) surrounding frequency shows agreement to within 2.0  $\mu$ as. However, Figure 3 (top) shows that the TPX08 model results in a 7  $\mu$ as reduction of residual variations at each of the two frequencies that are 0.0003 cpd away from the O<sub>1</sub> tidal component on both sides (higher and lower). These two frequencies do not correspond to known tidal terms. They appear to reflect systematic errors that manifest in the IERS 2010-based residual time series only, since their amplitudes are reduced to less than 1.2  $\mu$ as in the respective TPX08-based time series.

Figure 3 (middle and bottom panels) also shows prograde diurnal polar motion results from two additional cases, where the two considered background models of ocean tide effects are applied without the libration models. Corresponding results for semidiurnal prograde and retrograde polar motion are not explicitly shown because they agree to within the background noise level with the respective cases where the libration model was applied. This is expected because libration has no impact on semidiurnal polar motion. Most importantly, the application of the libration model together with the TPX08-based ocean tide model performs better than when the libration model is not applied, as evidenced by smaller amplitudes of the residual errors. In contrast, the IERS 2010 ocean tide model performs better, namely, has smaller residual errors, when the libration model is not simultaneously applied. This suggests that the TPX08-based model for ocean tide effects has better consistency with the libration model than does the IERS 2010 model.

The GPS-based time series provide an opportunity to consider residual errors in retrograde diurnal polar motion but should be interpreted with caution due to the inherent relationship to nutation and the challenge in observing nutation with satellite geodetic techniques [Rothacher *et al.*, 2001]. In the reference case (TPX08-based ocean tide with libration effects), the only tidal components with observed residual signal above 4  $\mu$ as are P<sub>1</sub>, S<sub>1</sub>, and K<sub>1</sub> with amplitudes of 7, 11, and 5  $\mu$ as, respectively. When using the IERS 2010 model instead,

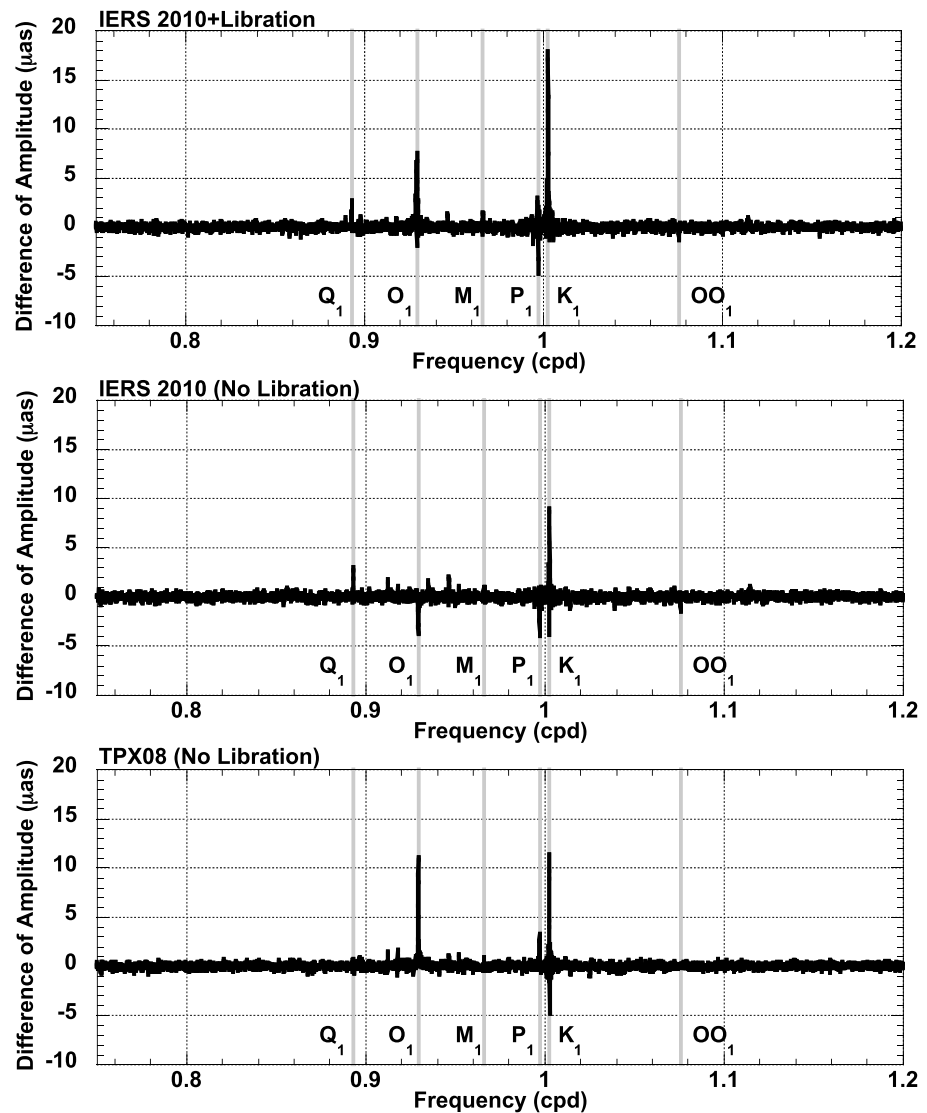


**Figure 3.** Differences of amplitude spectra of GPS-based observations of residual variations in prograde diurnal polar motion with respect to the spectrum shown in Figure 2 (top). Differences are for three respective background model cases: (top) IERS 2010 model for ocean tide effects with the *Mathews and Bretagnon* [2003] model for libration effects; (middle) IERS 2010 model for ocean tide effects without a model for libration effects; (bottom) this paper's TPX08-based model for ocean tide effects without a model for libration effects. Positive values indicate larger residual variations than when using the nominal TPX08-based model for ocean tide effects with the *Mathews and Bretagnon* [2003] model for libration effects, as shown in Figure 2. Gray lines indicate frequencies of some primary tidal components.

the respective amplitudes are very similar at 7, 10, and 7  $\mu\text{as}$ , respectively. This is as expected since the same nutation model has been used to generate the respective GPS-based residual time series.

#### 4. Conclusion

High-frequency GPS-based observations of polar motion are shown to provide an effective means to evaluate models of the predicted effects of the ocean tides and libration in the diurnal and semidiurnal tidal bands. These observations appear to be capable of discerning diurnal and semidiurnal variations with accuracies of 1–2  $\mu\text{as}$ . As such, they provide an additional approach to evaluating the long-wavelength components of global models of the ocean tide heights and currents [e.g., *Stammer et al.*, 2014]. The TPX08 ocean tide model, a more recent version of the model for the ocean tide effects that has been recommended by the IERS for the last two decades, shows two notable improvements over its predecessor. Residual polar

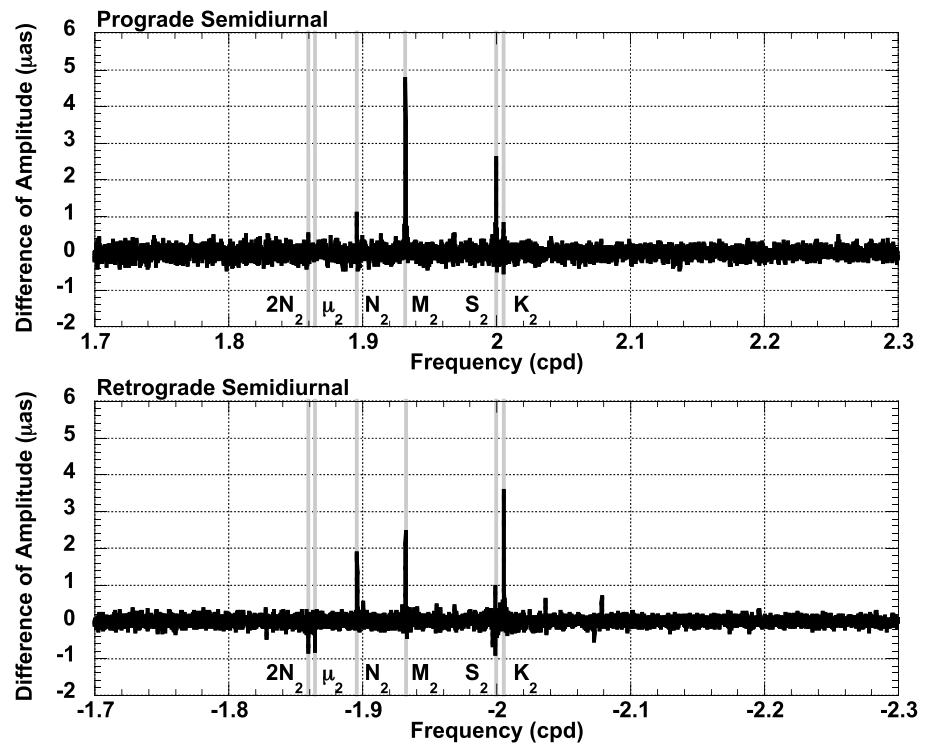


**Figure 4.** Differences of amplitude spectra of GPS-based observations of residual prograde and retrograde semidiurnal polar motion variations with respect to the spectra shown in Figures 2 (middle) and 2 (bottom). Differences are shown for (top) prograde and (bottom) retrograde semidiurnal polar motion, respectively. Both are for the approach that uses the IERS 2010 model for ocean tide effects with the *Mathews and Bretagnon* [2003] model for libration effects. Positive values indicate larger residual variations than when using the nominal TPX08-based model for ocean tide effects with the *Mathews and Bretagnon* [2003] model for libration effects, as shown in Figure 2. Libration effects have no substantive impact on the semidiurnal variation in polar motion, so the respective cases without a background libration model are not explicitly shown. Gray lines indicate frequencies of some primary tidal components.

motion variations at the primary tidal frequencies are, with the exception of  $P_1$ , always smaller when using the more recent model. Most significantly the residual signal at the  $K_1$  tidal frequency is smaller by  $16 \mu\text{as}$ . Residual tidal variations in polar motion are always below 10, 2, and  $5 \mu\text{as}$  for the prograde diurnal, prograde semidiurnal, and retrograde semidiurnal (except  $S_2$ ) tidal components, respectively. The residual signals at the primary tidal frequencies correspond to approximately 2–15% of the respective total predicted signal. In addition, the more recent model shows improved consistency with the conventional model for the effects of libration, again through smaller observed residual polar motion variations.

Nevertheless, some remaining weaknesses in the TPX08 ocean tide model and the approach in which we apply it to predicting EOP variations are observed. Residual variations for the  $P_1$  tide increase by  $5 \mu\text{as}$  compared to its predecessor. In addition, residual variations at those frequencies that lie on the outer edges of the tidal bands (e.g.,  $2N_2$ ,  $\mu_2$ , and  $OO_1$ ) have similar amplitudes to the respective total predicted effects. This suggests that the smooth response functions that we applied to the EOPs are particularly deficient when they are used to extrapolate, rather than interpolate, predicted variations from the explicitly provided primary tidal frequencies. The particular application of using ocean tide models to predict EOP variations is likely to benefit from explicit modeling of the tide heights and currents at frequencies on the outer edges of the respective tidal bands. However, the tide-generating potential at these frequencies is significantly smaller so the challenge lies with generating sufficiently accurate altimeter-based observations of the respective tide heights.

The high-frequency GPS-based polar motion observations appear to have accuracies that may prove beneficial to evaluating smaller, and previously ignored, effects on diurnal and semidiurnal polar motion. In particular, the effects of the atmosphere at the  $S_1$  and  $S_2$  tidal frequencies are at the level of the respective

observed residual tidal signals [Brzeziński *et al.*, 2004] and larger than the accuracies of the GPS observations. For those purposes, it would also become important to use a model for the observed  $S_1$  ocean tide [e.g., Ray and Egbert, 2004, Appendix A], as it includes a significant non-gravitational component. In addition, seasonal variations in the  $S_1$  atmospheric angular momentum will contribute to apparent EOP variations at the  $P_1$  and  $K_1$  tidal frequencies and are therefore also worth considering when investigating remaining residual polar motion variations. They may have some bearing on the observed increase in residual  $P_1$  polar motion variations when using the TPX08 model for ocean tide effects. The GPS observations might also lend insight into models for the impact of the triaxial core on libration effects [Brzeziński and Mathews, 2003], which have amplitudes similar to the accuracies of the GPS observations. Furthermore, the formulas that we have used to convert ocean tide angular momentum to predicted polar motion variations, from Sasao and Wahr [1981], may be worth revisiting with more recent Earth models. Similarly, the observed improvements in predicting tidal variations in polar motion from a modern ocean tide model are likely to also provide benefits to predicting the related effects on nutation.

## Appendix A: Earth Orientation Parameters Derived From Response Functions

Variants of smooth response assumptions are almost always used to determine the ocean tide response at frequencies that are not explicitly modeled. Specifically, the unit relative response in the frequency domain, often also referred to as the tidal admittance, is assumed to be smooth across some bandwidth [e.g., Munk and Cartwright, 1966]. This approach determines the tidal admittance by normalizing (i.e., dividing) the explicitly modeled tidal parameter, usually the tide heights and currents, by the respective tide-generating potential amplitude [e.g., Cartwright and Ray, 1990]. A smooth response function is then assumed and used to evaluate the tidal admittance at any frequency within the desired bandwidth. The tidal parameter at any frequency is then determined by rescaling (i.e., multiplying) the respective admittance by the associated tide-generating potential amplitude. We similarly apply the assumption of a smooth unit relative response to the EOPs. We assume smooth response functions for each of the three EOPs across each of the diurnal and semidiurnal tidal bands. The EOP predictions at the primary frequencies that are explicitly provided by the TPX08 tide model are used to derive the response functions.

We consider factors that might introduce non-negligible deviations from a smooth response when choosing the tidal frequencies that provide the source of the respective response functions. For example, the observed solar diurnal and semidiurnal,  $S_1$  and  $S_2$ , ocean tides include a response to the gravitational lunisolar tidal potential and a non-trivial response to non-gravitational effects such as atmospheric forcing [e.g., Ray and Egbert, 2004]. The observed  $K_1$  and  $K_2$  ocean tides are likely to also contain atmospheric effects but at significantly smaller level relative to the tidal gravitational effects. Here we assume that those non-gravitational effects at  $K_1$  and  $K_2$  can be ignored at least with regard to inferring the ocean tides at other smaller-amplitude tidal frequencies. Meanwhile, the free core nutation resonance is expected to cause deviations from a smooth response of the ocean tides at nearby diurnal frequencies. Desai and Wahr [1995] show that the free core nutation resonance is expected to amplify the effective ocean tide-generating potential, and therefore the response, of the  $K_1$  tide by 6% but by only 2% at the nearby  $P_1$  frequency. An additional consideration is the frequency separation between the tidal components that are used to derive the smooth response functions. For example, the  $K_1$  and  $P_1$  tidal components are only separated by 0.0055 cycles per day so there is limited value, if any, in having both contribute to determination of the response functions.

Given these considerations, we derive EOP response functions using the respective TPX08-based predicted variations for the  $Q_1$ ,  $O_1$ , and  $K_1$  tidal components in the diurnal band and  $N_2$ ,  $M_2$ , and  $K_2$  in the semidiurnal band. We use the free core nutation resonance functions from Desai and Wahr [1995, equations (20) and (22)] to determine the effective tide-generating potential amplitudes at the diurnal tidal frequencies when computing the unit response of the EOPs. Doing so mitigates the impact of the free core nutation resonance on the assumed diurnal response function. We use three independent parameters to define each of the diurnal and semidiurnal response functions, recognizing that we have predicted variations at only three independent frequencies in each tidal band. Of course, three-parameter response functions will exactly represent the predicted variations at those three frequencies. For the remaining two TPX08-based predicted EOP variations,  $S_2$  and  $P_1$ , we use values as explicitly computed from the tide model instead of those computed from the response functions.

**Table A1.** Coefficients of  $\sin(\theta(t))$  and  $\cos(\theta(t))$  of Diurnal and Semidiurnal Variations in Polar Motion,  $p_1$  and  $p_2$ , Caused by the Ocean Tides, Where  $\theta(t)$  Is the Astronomical Tidal Argument<sup>a</sup>

Tide	Tidal Argument, $\theta(t)$						Doodson Number	Period (days)	$p_1 (x_p)$		$p_2 (y_p)$	
	$\gamma$	$I$	$I'$	$F$	$D$	$\Omega$			sin	cos	sin	cos
2Q <sub>1</sub>	1	-2	0	-2	-2	-2	107.755	1.2670641	-0.11	0.24	-0.24	-0.11
	1	0	0	-2	-4	-2	109.555	1.2593143	-0.07	0.15	-0.15	-0.07
	1	-3	0	-2	0	-1	115.845	1.2187487	-0.03	0.10	-0.10	-0.03
	1	-3	0	-2	0	-2	115.855	1.2185303	-0.16	0.54	-0.54	-0.16
	1	-1	0	-2	-2	-1	117.645	1.2115770	-0.07	0.26	-0.26	-0.07
	1	-1	0	-2	-2	-2	117.655	1.2113611	-0.37	1.40	-1.40	-0.37
	1	-1	1	-2	-2	-2	118.654	1.2073570	-0.03	0.10	-0.10	-0.03
	1	1	0	-2	-4	-2	119.455	1.2042758	-0.06	0.27	-0.27	-0.06
	1	-2	0	-2	0	-1	125.745	1.1671263	-0.04	0.83	-0.83	-0.04
	1	-2	0	-2	0	-2	125.755	1.1669259	-0.19	4.41	-4.41	-0.19
$\sigma_1$	1	0	0	-2	-2	-1	127.545	1.1605476	-0.01	0.99	-0.99	-0.01
	1	0	0	-2	-2	-2	127.555	1.1603495	-0.03	5.24	-5.24	-0.03
	1	0	1	-2	-2	-2	128.554	1.1566750	0.01	0.35	-0.35	0.01
	1	2	0	-2	-4	-2	129.355	1.1538467	0.00	0.16	-0.16	0.00
	1	-3	0	-2	2	-2	133.855	1.1256354	-0.02	-0.09	0.09	-0.02
	1	-1	-1	-2	0	-2	134.656	1.1229567	-0.05	-0.25	0.25	-0.05
	1	1	0	-4	0	-2	135.435	1.1206604	-0.03	-0.11	0.11	-0.03
	1	-1	0	-2	0	0	135.635	1.1198837	-0.04	-0.17	0.17	-0.04
	1	-1	0	-2	0	-1	135.645	1.1196992	1.33	5.46	-5.46	1.33
	1	-1	0	-2	0	-2	135.655	1.1195149	7.08	28.95	-28.95	7.08
Q <sub>1</sub>	1	0	0	-2	-1	-2	136.555	1.1164795	-0.04	-0.15	0.15	-0.04
	1	-1	1	-2	0	-2	136.654	1.1160941	0.07	0.27	-0.27	0.07
	1	1	0	-2	-2	-1	137.445	1.1136429	0.29	1.01	-1.01	0.29
	1	1	0	-2	-2	-2	137.455	1.1134606	1.53	5.38	-5.38	1.53
	1	-1	0	0	-2	0	137.655	1.1126938	-0.09	-0.31	0.31	-0.09
	1	-1	0	0	-2	-1	137.665	1.1125117	0.03	0.10	-0.10	0.03
	1	1	1	-2	-2	-2	138.454	1.1100766	0.07	0.24	-0.24	0.07
	1	-2	0	-2	2	-2	143.755	1.0814566	-0.20	-0.39	0.39	-0.20
	1	0	-1	-2	0	-2	144.556	1.0789839	-0.23	-0.44	0.44	-0.23
	1	0	0	-2	0	0	145.535	1.0761465	-0.39	-0.73	0.73	-0.39
$\rho_1$	1	0	0	-2	0	-1	145.545	1.0759762	12.84	23.85	-23.85	12.84
	1	0	0	-2	0	-2	145.555	1.0758059	68.16	126.32	-126.32	68.16
	1	-2	0	0	0	0	145.755	1.0750901	-0.44	-0.81	0.81	-0.44
	1	-2	0	0	0	-1	145.765	1.0749201	-0.07	-0.13	0.13	-0.07
	1	0	1	-2	0	-2	146.554	1.0726466	0.21	0.38	-0.38	0.21
	1	0	0	0	-2	0	147.555	1.0695055	-0.93	-1.60	1.60	-0.93
	1	0	0	0	-2	-1	147.565	1.0693373	0.20	0.35	-0.35	0.20
	1	0	1	0	-2	0	148.554	1.0663831	-0.06	-0.10	0.10	-0.06
	1	-1	0	-2	2	-1	153.645	1.0407740	-0.13	-0.18	0.18	-0.13
	1	-1	0	-2	2	-2	153.655	1.0406147	-0.59	-0.79	0.79	-0.59
$\tau_1$	1	1	0	-2	0	-1	155.445	1.0355394	-0.42	-0.55	0.55	-0.42
	1	1	0	-2	0	-2	155.455	1.0353817	-2.26	-2.96	2.96	-2.26
	1	-1	0	0	0	1	155.645	1.0348762	0.18	0.24	-0.24	0.18
	1	-1	0	0	0	0	155.655	1.0347187	-6.28	-8.22	8.22	-6.28
	1	-1	0	0	0	-1	155.665	1.0345612	-1.26	-1.65	1.65	-1.26
	1	1	0	0	-2	0	157.455	1.0295447	-1.20	-1.54	1.54	-1.20
	1	1	0	0	-2	-1	157.465	1.0293888	-0.26	-0.34	0.34	-0.26
	1	0	-2	-2	2	-2	161.557	1.0082815	0.08	0.10	-0.10	0.08
	1	0	-1	-2	2	-2	162.556	1.0055058	2.02	2.55	-2.55	2.02
	1	0	0	-2	2	-1	163.545	1.0028934	-0.38	-0.49	0.49	-0.38
P <sub>1</sub>	1	0	0	-2	2	-2	163.555	1.0027454	30.11	42.73	-42.73	30.11
	1	0	1	-2	2	-2	164.554	1.0000001	-0.28	-0.36	0.36	-0.28
	1	0	-1	0	0	0	164.556	0.9999999	-0.80	-1.03	1.03	-0.80
	1	0	0	0	0	1	165.545	0.9974159	2.03	2.65	-2.65	2.03
	1	0	0	0	0	0	165.555	0.9972696	-102.68	-134.45	134.45	-102.68
	1	0	0	0	0	-1	165.565	0.9971233	-13.97	-18.30	18.30	-13.97
	1	0	0	0	0	-2	165.575	0.9969771	0.30	0.39	-0.39	0.30
	1	0	1	0	0	0	166.554	0.9945541	-0.49	-0.65	0.65	-0.49
	1	0	0	2	-2	2	167.555	0.9918532	-1.25	-1.70	1.70	-1.25
	1	0	0	2	-2	2	167.555	0.9918532	-1.25	-1.70	1.70	-1.25

Table A1. (continued)

Tide	Tidal Argument, $\theta(t)$						Doodson Number	Period (days)	$p_1 (x_p)$		$p_2 (y_p)$	
	$\gamma$	$l$	$l'$	$F$	$D$	$\Omega$			sin	cos	sin	cos
$\theta_1$	1	0	1	2	-2	2	168.554	0.9891671	-0.07	-0.10	0.10	-0.07
	1	-1	0	0	2	0	173.655	0.9669565	-0.65	-1.30	1.30	-0.65
	1	-1	0	0	2	-1	173.665	0.9668190	-0.13	-0.26	0.26	-0.13
$J_1$	1	1	0	0	0	1	175.445	0.9625728	0.09	0.20	-0.20	0.09
	1	1	0	0	0	0	175.455	0.9624365	-3.01	-6.81	6.81	-3.01
	1	1	0	0	0	-1	175.465	0.9623003	-0.60	-1.35	1.35	-0.60
	1	-1	0	2	0	2	175.655	0.9618636	0.05	0.10	-0.10	0.05
	1	0	-1	0	2	0	182.556	0.9365694	0.00	-0.08	0.08	0.00
$SO_1$	1	0	0	0	2	0	183.555	0.9341741	-0.01	-1.21	1.21	-0.01
	1	0	0	0	2	-1	183.565	0.9340457	0.00	-0.24	0.24	0.00
	1	2	0	0	0	0	185.355	0.9299547	0.03	-0.61	0.61	0.03
$OO_1$	1	2	0	0	0	-1	185.365	0.9298275	0.01	-0.12	0.12	0.01
	1	0	0	2	0	2	185.555	0.9294198	0.27	-4.09	4.09	0.27
	1	0	0	2	0	1	185.565	0.9292927	0.18	-2.62	2.62	0.18
	1	0	0	2	0	0	185.575	0.9291657	0.04	-0.55	0.55	0.04
	1	1	0	0	2	0	193.455	0.9035416	0.10	-0.23	0.23	0.10
$v_1$	1	-1	0	2	2	2	193.655	0.9030366	0.08	-0.17	0.17	0.08
	1	-1	0	2	2	1	193.665	0.9029166	0.05	-0.11	0.11	0.05
	1	3	0	0	0	0	195.255	0.8995938	0.03	-0.06	0.06	0.03
	1	1	0	2	0	2	195.455	0.8990932	0.45	-0.93	0.93	0.45
	1	1	0	2	0	1	195.465	0.8989743	0.29	-0.60	0.60	0.29
	1	1	0	2	0	0	195.475	0.8988554	0.06	-0.13	0.13	0.06
	1	0	0	2	2	2	1X3.555	0.8743808	0.12	-0.18	0.18	0.12
	1	0	0	2	2	1	1X3.565	0.8742683	0.08	-0.11	0.11	0.08
	1	2	0	2	0	2	1X5.355	0.8706832	0.11	-0.15	0.15	0.11
	1	2	0	2	0	1	1X5.365	0.8705717	0.07	-0.10	0.10	0.07
	1	1	0	2	2	2	1E3.455	0.8474877	0.04	-0.05	0.05	0.04
	2	-4	0	-2	0	-2	215.955	0.5595636	-0.01	0.04	0.09	0.01
	2	-2	0	-2	-2	-2	217.755	0.5580469	-0.07	0.15	0.36	0.06
	2	0	0	-2	-4	-2	219.555	0.5565385	-0.05	0.08	0.21	0.04
	2	-3	0	-2	0	-2	225.855	0.5484264	-0.35	0.13	0.60	0.22
$\varepsilon_2$	2	-1	0	-2	-2	-2	227.655	0.5469695	-0.98	0.25	1.46	0.61
	2	-1	1	-2	-2	-2	228.654	0.5461516	-0.08	0.02	0.11	0.05
	2	1	0	-2	-4	-2	229.455	0.5455203	-0.20	0.03	0.26	0.12
	2	-2	-1	-2	0	-2	234.756	0.5385167	0.07	0.01	-0.04	-0.04
	2	-2	0	-2	0	-1	235.745	0.5377665	0.19	0.02	-0.12	-0.11
$2N_2$	2	-2	0	-2	0	-2	235.755	0.5377239	-5.17	-0.5	3.14	2.97
	2	0	-1	-2	-2	-2	236.556	0.5371119	0.09	0.01	-0.05	-0.05
	2	-2	1	-2	0	-2	236.754	0.5369335	-0.08	-0.01	0.05	0.05
$\mu_2$	2	0	0	-2	-2	-1	237.545	0.5363655	0.25	0.03	-0.13	-0.14
	2	0	0	-2	-2	-2	237.555	0.5363232	-6.57	-0.79	3.49	3.76
	2	0	1	-2	-2	-2	238.554	0.5355369	-0.46	-0.06	0.22	0.26
	2	2	0	-2	-4	-2	239.355	0.5349298	-0.21	-0.03	0.10	0.12
	2	-3	0	-2	2	-2	243.855	0.5287858	0.17	0.03	-0.04	-0.09
$N_2$	2	-1	-1	-2	0	-2	244.656	0.5281939	0.44	0.07	-0.11	-0.25
	2	1	0	-4	0	-2	245.435	0.5276853	0.20	0.03	-0.05	-0.12
	2	-1	0	-2	0	-1	245.645	0.5274721	1.98	0.33	-0.47	-1.13
	2	-1	0	-2	0	-2	245.655	0.5274312	-53.18	-8.81	12.56	30.30
	2	1	-1	-2	-2	-2	246.456	0.5268423	0.10	0.02	-0.02	-0.06
	2	0	0	-2	-1	-2	246.555	0.5267565	0.29	0.05	-0.07	-0.17
	2	-1	1	-2	0	-2	246.654	0.5266707	-0.51	-0.08	0.11	0.29
	2	1	0	-2	-2	-1	247.445	0.5261242	0.39	0.06	-0.08	-0.22
	2	1	0	-2	-2	-2	247.455	0.5260835	-10.40	-1.68	2.20	5.94
	2	1	1	-2	-2	-2	248.454	0.5253269	-0.49	-0.08	0.10	0.28
$v_2$	2	0	0	-4	2	-2	253.535	0.5190751	0.14	0.01	-0.02	-0.08
	2	-2	0	-2	2	-2	253.755	0.5188292	0.97	0.10	-0.14	-0.56
	2	0	-1	-2	0	-2	254.556	0.5182594	1.12	0.11	-0.16	-0.65
	2	0	0	-2	0	0	255.535	0.5176039	-0.17	-0.02	0.02	0.10
	2	0	0	-2	0	-1	255.545	0.5175644	12.19	1.08	-1.74	-7.14
	2	0	0	-2	0	-2	255.555	0.5175251	-326.96	-28.72	46.64	191.61

Table A1. (continued)

Tide	Tidal Argument, $\theta(t)$						Doodson Number	Period (days)	$p_1 (x_p)$		$p_2 (y_p)$	
	$\gamma$	$l$	$l'$	$F$	$D$	$\Omega$			sin	cos	sin	cos
$\lambda_2$	2	-2	0	0	0	0	255.755	0.5173593	-0.19	-0.02	0.03	0.11
	2	0	1	-2	0	-2	256.554	0.5167928	-1.00	-0.08	0.14	0.59
	2	2	0	-2	-2	-2	257.355	0.5162275	0.19	0.01	-0.03	-0.11
	2	0	0	0	-2	0	257.555	0.5160626	-0.39	-0.03	0.06	0.23
	2	0	0	0	-2	-1	257.565	0.5160234	0.19	0.01	-0.03	-0.11
	2	-1	-1	-2	2	-2	262.656	0.5099516	0.12	0.00	-0.02	-0.07
	2	-1	0	-2	2	-1	263.645	0.5092787	-0.11	0.01	0.02	0.07
	2	-1	0	-2	2	-2	263.655	0.5092406	2.52	-0.14	-0.48	-1.54
	2	1	0	-2	0	-1	265.445	0.5080221	-0.35	0.03	0.07	0.22
	2	1	0	-2	0	-2	265.455	0.5079842	9.66	-0.81	-2.00	-5.95
$L_2$	2	-1	0	0	0	0	265.655	0.5078245	-2.42	0.21	0.51	1.49
	2	-1	0	0	0	-1	265.665	0.5077866	-1.07	0.09	0.22	0.66
	2	-1	0	0	0	-2	265.675	0.5077487	-0.15	0.01	0.03	0.09
	2	1	0	0	-2	0	267.455	0.5065751	-0.46	0.05	0.11	0.29
	2	1	0	0	-2	-1	267.465	0.5065373	-0.22	0.03	0.05	0.14
	2	0	-2	-2	2	-2	271.557	0.5013726	-0.36	0.10	0.12	0.23
	2	0	-1	-2	2	-2	272.556	0.5006854	-8.89	2.57	3.20	5.78
	2	0	0	-2	2	-1	273.545	0.5000368	-0.34	0.11	0.13	0.22
	2	0	0	-2	2	-2	273.555	0.5000000	-134.55	69.53	70.34	85.37
	2	0	1	-2	2	-2	274.554	0.4993165	1.25	-0.42	-0.50	-0.82
$S_2$	2	0	-1	0	0	0	274.556	0.4993164	-0.32	0.11	0.13	0.21
	2	0	0	0	0	1	275.545	0.4986714	0.52	-0.19	-0.22	-0.34
	2	0	0	0	0	0	275.555	0.4986348	-40.28	14.62	17.05	26.66
	2	0	0	0	0	-1	275.565	0.4985982	-12.00	4.37	5.09	7.95
	2	0	0	0	0	-2	275.575	0.4985616	-1.30	0.48	0.55	0.86
	2	0	1	0	0	0	276.554	0.4979550	-0.31	0.12	0.14	0.21
	2	0	0	2	-2	2	277.555	0.4972770	-0.27	0.11	0.13	0.18
	2	-1	0	0	2	0	283.655	0.4909396	-0.37	0.27	0.28	0.26
	2	-1	0	0	2	-1	283.665	0.4909041	-0.16	0.12	0.12	0.12
	2	1	0	0	0	0	285.455	0.4897717	-1.86	1.50	1.58	1.36
$\eta_2$	2	1	0	0	0	-1	285.465	0.4897365	-0.81	0.65	0.69	0.59
	2	1	0	0	0	-2	285.475	0.4897012	-0.09	0.07	0.08	0.07
	2	0	0	0	2	0	293.555	0.4823456	-0.23	0.34	0.36	0.19
	2	0	0	0	2	-1	293.565	0.4823114	-0.10	0.15	0.15	0.08
	2	2	0	0	0	0	295.355	0.4812183	-0.11	0.17	0.19	0.09
	2	0	0	2	0	2	295.555	0.4810750	-0.34	0.56	0.59	0.29
	2	0	0	2	0	1	295.565	0.4810409	-0.29	0.48	0.51	0.25
	2	0	0	2	0	0	295.575	0.4810069	-0.10	0.16	0.17	0.08
	2	1	0	2	0	2	2X5.455	0.4728200	-0.04	0.13	0.14	0.04
	2	1	0	2	0	1	2X5.465	0.4727871	-0.03	0.11	0.12	0.04

<sup>a</sup>The units are  $\mu\text{s}$ .  $\gamma$  denotes Greenwich Mean Sidereal Time +  $\pi$ . Values are based upon ocean tide angular momentum predictions at the eight primary diurnal and semidiurnal tidal frequencies from the TPX08 ocean tide model, followed by a smooth response assumption at other tidal frequencies. Digits X and E in Doodson numbers represent values of 10 and 11, respectively.

We choose to parameterize the EOP response functions by the Fourier series shown in equation (5). The coefficients  $A$ ,  $B$ , and  $C$  are independently computed for each of the diurnal and semidiurnal tidal bands, for each EOP (e.g.,  $p_1$ ,  $p_2$ , and LOD), and each of the associated in-phase and quadrature components, using the tidal frequencies mentioned above.

$$f(\omega) = A + B\cos\omega\tau + C\sin\omega\tau. \quad (5)$$

This approach is motivated by the so-called convolution formalism of *Munk and Cartwright* [1966]. We also adopt their Fourier series period of  $2\pi/\tau$ , with  $\tau = 2$  days. It is worth mentioning that the *Groves and Reynolds* [1975] orthotide approach was applied to determine the ocean tide EOP response functions for the current IERS conventions [*Petit and Luzum*, 2010]. In the frequency domain, the convolution, orthotide, and Fourier series approaches are functionally equivalent when using the same number of Fourier series terms. The orthotide approach simply provides basis functions that are orthogonal in the time domain but that are

**Table A2.** Coefficients of  $\sin(\theta(t))$  and  $\cos(\theta(t))$  of Diurnal and Semidiurnal Variations in UT1 and Length-of-Day (LOD) Caused by the Ocean Tides, Where  $\theta(t)$  is the Astronomical Tidal Argument<sup>a</sup>

Tide	Tidal Argument, $\theta(t)$						Doodson Number	Period (days)	UT1		LOD	
	$\gamma$	$I$	$I'$	$F$	$D$	$\Omega$			sin	cos	sin	cos
2Q <sub>1</sub>	1	-2	0	-2	-2	-2	107.755	1.2670641	0.07	-0.01	-0.05	-0.34
	1	0	0	-2	-4	-2	109.555	1.2593143	0.04	-0.01	-0.03	-0.21
	1	-3	0	-2	0	-1	115.845	1.2187487	0.03	-0.01	-0.03	-0.13
	1	-3	0	-2	0	-2	115.855	1.2185303	0.14	-0.03	-0.15	-0.71
	1	-1	0	-2	-2	-1	117.645	1.2115770	0.07	-0.02	-0.08	-0.34
	1	-1	0	-2	-2	-2	117.655	1.2113611	0.35	-0.08	-0.42	-1.80
	1	-1	1	-2	-2	-2	118.654	1.2073570	0.03	-0.01	-0.03	-0.13
	1	1	0	-2	-4	-2	119.455	1.2042758	0.06	-0.02	-0.08	-0.34
	1	-2	0	-2	0	-1	125.745	1.1671263	0.18	-0.06	-0.33	-0.95
	1	-2	0	-2	0	-2	125.755	1.1669259	0.94	-0.32	-1.74	-5.05
$\sigma_1$	1	0	0	-2	-2	-1	127.545	1.1605476	0.20	-0.07	-0.40	-1.11
	1	0	0	-2	-2	-2	127.555	1.1603495	1.08	-0.40	-2.14	-5.86
	1	0	1	-2	-2	-2	128.554	1.1566750	0.07	-0.03	-0.15	-0.39
	1	2	0	-2	-4	-2	129.355	1.1538467	0.03	-0.01	-0.07	-0.17
	1	-3	0	-2	2	-2	133.855	1.1256354	-0.02	0.01	0.05	0.09
	1	-1	-1	-2	0	-2	134.656	1.1229567	-0.04	0.02	0.12	0.24
	1	1	0	-4	0	-2	135.435	1.1206604	-0.02	0.01	0.06	0.11
	1	-1	0	-2	0	0	135.635	1.1198837	-0.03	0.01	0.08	0.16
	1	-1	0	-2	0	-1	135.645	1.1196992	0.92	-0.49	-2.73	-5.17
	1	-1	0	-2	0	-2	135.655	1.1195149	4.88	-2.58	-14.48	-27.39
Q <sub>1</sub>	1	0	0	-2	-1	-2	136.555	1.1164795	-0.03	0.01	0.08	0.14
	1	-1	1	-2	0	-2	136.654	1.1160941	0.04	-0.02	-0.14	-0.25
	1	1	0	-2	-2	-1	137.445	1.1136429	0.17	-0.09	-0.52	-0.93
	1	1	0	-2	-2	-2	137.455	1.1134606	0.88	-0.49	-2.76	-4.94
	1	-1	0	0	-2	0	137.655	1.1126938	-0.05	0.03	0.16	0.28
	1	-1	0	0	-2	-1	137.665	1.1125117	0.02	-0.01	-0.05	-0.09
	1	1	1	-2	-2	-2	138.454	1.1100766	0.04	-0.02	-0.13	-0.22
	1	-2	0	-2	2	-2	143.755	1.0814566	-0.05	0.04	0.22	0.30
	1	0	-1	-2	0	-2	144.556	1.0789839	-0.06	0.04	0.25	0.34
	1	0	0	-2	0	0	145.535	1.0761465	-0.09	0.07	0.42	0.55
O <sub>1</sub>	1	0	0	-2	0	-1	145.545	1.0759762	3.06	-2.37	-13.83	-17.86
	1	0	0	-2	0	-2	145.555	1.0758059	16.18	-12.55	-73.30	-94.50
	1	-2	0	0	0	0	145.755	1.0750901	-0.10	0.08	0.47	0.60
	1	-2	0	0	0	-1	145.765	1.0749201	-0.02	0.01	0.08	0.10
	1	0	1	-2	0	-2	146.554	1.0726466	0.05	-0.04	-0.22	-0.28
	1	0	0	0	-2	0	147.555	1.0695055	-0.20	0.16	0.94	1.16
	1	0	0	0	-2	-1	147.565	1.0693373	0.04	-0.03	-0.20	-0.25
	1	0	1	0	-2	0	148.554	1.0663831	-0.01	0.01	0.06	0.07
	1	-1	0	-2	2	-1	153.645	1.0407740	-0.02	0.02	0.11	0.11
	1	-1	0	-2	2	-2	153.655	1.0406147	-0.08	0.08	0.47	0.51
$\tau_1$	1	1	0	-2	0	-1	155.445	1.0355394	-0.06	0.05	0.32	0.35
	1	1	0	-2	0	-2	155.455	1.0353817	-0.31	0.29	1.74	1.88
	1	-1	0	0	0	1	155.645	1.0348762	0.02	-0.02	-0.14	-0.15
	1	-1	0	0	0	0	155.655	1.0347187	-0.86	0.79	4.83	5.22
	1	-1	0	0	0	-1	155.665	1.0345612	-0.17	0.16	0.97	1.05
	1	1	0	0	-2	0	157.455	1.0295447	-0.16	0.15	0.89	0.98
	1	1	0	0	-2	-1	157.465	1.0293888	-0.04	0.03	0.20	0.21
	1	0	-2	-2	2	-2	161.557	1.0082815	0.01	-0.01	-0.05	-0.07
	1	0	-1	-2	2	-2	162.556	1.0055058	0.29	-0.21	-1.29	-1.80
	1	0	0	-2	2	-1	163.545	1.0028934	-0.06	0.04	0.24	0.35
P <sub>1</sub>	1	0	0	-2	2	-2	163.555	1.0027454	5.22	-3.08	-19.3	-32.71
	1	0	1	-2	2	-2	164.554	1.0000001	-0.04	0.03	0.17	0.27
	1	0	-1	0	0	0	164.556	0.9999999	-0.12	0.08	0.49	0.76
	1	0	0	0	0	1	165.545	0.9974159	0.32	-0.20	-1.24	-2.02
	1	0	0	0	0	0	165.555	0.9972696	-16.29	9.95	62.69	102.63
	1	0	0	0	0	-1	165.565	0.9971233	-2.22	1.35	8.52	13.99
	1	0	0	0	0	-2	165.575	0.9969771	0.05	-0.03	-0.18	-0.30
	1	0	1	0	0	0	166.554	0.9945541	-0.08	0.05	0.29	0.51
	1	0	0	2	-2	2	167.555	0.9918532	-0.22	0.12	0.74	1.38
	1	0	0	2	-2	2	167.555	0.9918532	-0.22	0.12	0.74	1.38

Table A2. (continued)

Tide	Tidal Argument, $\theta(t)$						Doodson Number	Period (days)	UT1		LOD	
	$\gamma$	$I$	$I'$	$F$	$D$	$\Omega$			sin	cos	sin	cos
$\theta_1$	1	0	1	2	-2	2	168.554	0.9891671	-0.01	0.01	0.04	0.08
	1	-1	0	0	2	0	173.655	0.9669565	-0.23	0.05	0.34	1.48
	1	-1	0	0	2	-1	173.665	0.9668190	-0.05	0.01	0.07	0.29
$J_1$	1	1	0	0	0	1	175.445	0.9625728	0.04	-0.01	-0.05	-0.24
	1	1	0	0	0	0	175.455	0.9624365	-1.26	0.24	1.54	8.25
	1	1	0	0	0	-1	175.465	0.9623003	-0.25	0.05	0.30	1.64
$SO_1$	1	-1	0	2	0	2	175.655	0.9618636	0.02	0.00	-0.02	-0.13
	1	0	-1	0	2	0	182.556	0.9365694	-0.02	0.00	0.00	0.13
	1	0	0	0	2	0	183.555	0.9341741	-0.31	0.00	0.02	2.10
$OO_1$	1	0	0	0	2	-1	183.565	0.9340457	-0.06	0.00	0.00	0.41
	1	2	0	0	0	0	185.355	0.9299547	-0.16	0.00	-0.01	1.11
	1	2	0	0	0	-1	185.365	0.9298275	-0.03	0.00	0.00	0.22
$v_1$	1	0	0	2	0	2	185.555	0.9294198	-1.10	-0.01	-0.07	7.44
	1	0	0	2	0	1	185.565	0.9292927	-0.71	-0.01	-0.05	4.77
	1	0	0	2	0	0	185.575	0.9291657	-0.15	0.00	-0.01	1.00
$\varepsilon_2$	1	1	0	0	2	0	193.455	0.9035416	-0.07	0.00	-0.03	0.51
	1	-1	0	2	2	2	193.655	0.9030366	-0.06	0.00	-0.02	0.39
	1	-1	0	2	2	1	193.665	0.9029166	-0.04	0.00	-0.01	0.25
$2N_2$	1	3	0	0	0	0	195.255	0.8995938	-0.02	0.00	-0.01	0.13
	1	1	0	2	0	2	195.455	0.8990932	-0.31	-0.02	-0.13	2.13
	1	1	0	2	0	1	195.465	0.8989743	-0.20	-0.01	-0.08	1.37
$\mu_2$	1	1	0	2	0	0	195.475	0.8988554	-0.04	0.00	-0.02	0.29
	1	0	0	2	2	2	1X3.555	0.8743808	-0.06	0.00	-0.03	0.44
	1	0	0	2	2	1	1X3.565	0.8742683	-0.04	0.00	-0.02	0.28
$N_2$	1	2	0	2	0	2	1X5.355	0.8706832	-0.05	0.00	-0.02	0.38
	1	2	0	2	0	1	1X5.365	0.8705717	-0.03	0.00	-0.01	0.24
	1	1	0	2	2	2	1E3.455	0.8474877	-0.02	0.00	0.00	0.13
$2N_2$	2	-4	0	-2	0	-2	215.955	0.5595636	-0.01	0.00	0.00	0.12
	2	-2	0	-2	-2	-2	217.755	0.5580469	-0.04	0.00	-0.01	0.50
	2	0	0	-2	-4	-2	219.555	0.5565385	-0.03	0.00	-0.01	0.30
$\varepsilon_2$	2	-3	0	-2	0	-2	225.855	0.5484264	-0.09	-0.01	-0.13	1.02
	2	-1	0	-2	-2	-2	227.655	0.5469695	-0.03	-0.38	2.58	1.01
	2	-1	1	-2	-2	-2	228.654	0.5461516	-0.02	0.00	-0.03	0.19
$2N_2$	2	1	0	-2	-4	-2	229.455	0.5455203	-0.04	-0.01	-0.08	0.49
	2	-2	-1	-2	0	-2	234.756	0.5385167	0.01	0.00	0.03	-0.10
	2	-2	0	-2	0	-1	235.745	0.5377665	0.02	0.01	0.08	-0.28
$\mu_2$	2	-2	0	-2	0	-2	235.755	0.5377239	-0.64	-0.18	-2.10	7.45
	2	0	-1	-2	-2	-2	236.556	0.5371119	0.01	0.00	0.04	-0.13
	2	-2	1	-2	0	-2	236.754	0.5369335	-0.01	0.00	-0.03	0.11
$N_2$	2	0	0	-2	-2	-1	237.545	0.5363655	0.03	0.01	0.10	-0.33
	2	0	0	-2	-2	-2	237.555	0.5363232	-0.75	-0.23	-2.65	8.74
	2	0	1	-2	-2	-2	238.554	0.5355369	-0.05	-0.02	-0.18	0.58
$v_2$	2	2	0	-2	-4	-2	239.355	0.5349298	-0.02	-0.01	-0.08	0.26
	2	-3	0	-2	2	-2	243.855	0.5287858	0.01	0.01	0.06	-0.15
	2	-1	-1	-2	0	-2	244.656	0.5281939	0.03	0.01	0.16	-0.39
$N_2$	2	1	0	-4	0	-2	245.435	0.5276853	0.01	0.01	0.07	-0.18
	2	-1	0	-2	0	-1	245.645	0.5274721	0.14	0.06	0.73	-1.71
	2	-1	0	-2	0	-2	245.655	0.5274312	-3.84	-1.64	-19.54	45.75
$M_2$	2	1	-1	-2	-2	-2	246.456	0.5268423	0.01	0.00	0.04	-0.08
	2	0	0	-2	-1	-2	246.555	0.5267565	0.02	0.01	0.11	-0.24
	2	-1	1	-2	0	-2	246.654	0.5266707	-0.04	-0.02	-0.18	0.42
$v_2$	2	1	0	-2	-2	-1	247.445	0.5261242	0.03	0.01	0.14	-0.32
	2	1	0	-2	-2	-2	247.455	0.5260835	-0.71	-0.31	-3.74	8.47
	2	1	1	-2	-2	-2	248.454	0.5253269	-0.03	-0.01	-0.17	0.39
$M_2$	2	0	0	-4	2	-2	253.535	0.5190751	0.01	0.00	0.04	-0.09
	2	-2	0	-2	2	-2	253.755	0.5188292	0.05	0.02	0.30	-0.63
	2	0	-1	-2	0	-2	254.556	0.5182594	0.06	0.03	0.34	-0.71
$M_2$	2	0	0	-2	0	0	255.535	0.5176039	-0.01	0.00	-0.05	0.11
	2	0	0	-2	0	-1	255.545	0.5175644	0.63	0.30	3.68	-7.68
	2	0	0	-2	0	-2	255.555	0.5175251	-16.94	-8.11	-98.46	205.67

Table A2. (continued)

Tide	Tidal Argument, $\theta(t)$						Doodson Number	Period (days)	UT1		LOD	
	$\gamma$	$I$	$I'$	$F$	$D$	$\Omega$			sin	cos	sin	cos
$\lambda_2$	2	-2	0	0	0	0	255.755	0.5173593	-0.01	0.00	-0.06	0.12
	2	0	1	-2	0	-2	256.554	0.5167928	-0.05	-0.02	-0.29	0.62
	2	2	0	-2	-2	-2	257.355	0.5162275	0.01	0.00	0.05	-0.12
	2	0	0	0	-2	0	257.555	0.5160626	-0.02	-0.01	-0.11	0.24
	2	0	0	0	-2	-1	257.565	0.5160234	0.01	0.00	0.05	-0.11
	2	-1	-1	-2	2	-2	262.656	0.5099516	0.01	0.00	0.03	-0.07
	2	-1	0	-2	2	-1	263.645	0.5092787	-0.01	0.00	-0.03	0.07
	2	-1	0	-2	2	-2	263.655	0.5092406	0.12	0.05	0.57	-1.49
	2	1	0	-2	0	-1	265.445	0.5080221	-0.02	-0.01	-0.07	0.21
	2	1	0	-2	0	-2	265.455	0.5079842	0.46	0.16	2.04	-5.75
$L_2$	2	-1	0	0	0	0	265.655	0.5078245	-0.12	-0.04	-0.51	1.44
	2	-1	0	0	0	-1	265.665	0.5077866	-0.05	-0.02	-0.22	0.64
	2	-1	0	0	0	-2	265.675	0.5077487	-0.01	0.00	-0.03	0.09
	2	1	0	0	-2	0	267.455	0.5065751	-0.02	-0.01	-0.09	0.28
	2	1	0	0	-2	-1	267.465	0.5065373	-0.01	0.00	-0.04	0.13
	2	0	-2	-2	2	-2	271.557	0.5013726	-0.02	0.00	-0.05	0.25
	2	0	-1	-2	2	-2	272.556	0.5006854	-0.49	-0.08	-1.04	6.14
	2	0	0	-2	2	-1	273.545	0.5000368	-0.02	0.00	-0.04	0.24
	2	0	0	-2	2	-2	273.555	0.5000000	-8.44	-0.71	-8.92	106.06
	2	0	1	-2	2	-2	274.554	0.4993165	0.07	0.01	0.12	-0.91
$S_2$	2	0	-1	0	0	0	274.556	0.4993164	-0.02	0.00	-0.03	0.23
	2	0	0	0	0	1	275.545	0.4986714	0.03	0.00	0.04	-0.38
	2	0	0	0	0	0	275.555	0.4986348	-2.37	-0.27	-3.40	29.86
	2	0	0	0	0	-1	275.565	0.4985982	-0.71	-0.08	-1.01	8.91
	2	0	0	0	0	-2	275.575	0.4985616	-0.08	-0.01	-0.11	0.97
	2	0	1	0	0	0	276.554	0.4979550	-0.02	0.00	-0.02	0.24
	2	0	0	2	-2	2	277.555	0.4972770	-0.02	0.00	-0.02	0.21
	2	-1	0	0	2	0	283.655	0.4909396	-0.03	0.00	0.03	0.39
	2	-1	0	0	2	-1	283.665	0.4909041	-0.01	0.00	0.01	0.17
	2	1	0	0	0	0	285.455	0.4897717	-0.16	0.01	0.19	2.11
$\zeta_2$	2	1	0	0	0	-1	285.465	0.4897365	-0.07	0.01	0.08	0.92
	2	1	0	0	0	-2	285.475	0.4897012	-0.01	0.00	0.01	0.10
	2	0	0	0	2	0	293.555	0.4823456	-0.03	0.01	0.09	0.43
	2	0	0	0	2	-1	293.565	0.4823114	-0.01	0.00	0.04	0.19
	2	2	0	0	0	0	295.355	0.4812183	-0.02	0.00	0.05	0.22
	2	0	0	2	0	2	295.555	0.4810750	-0.05	0.01	0.15	0.71
	2	0	0	2	0	1	295.565	0.4810409	-0.05	0.01	0.13	0.61
	2	0	0	2	0	0	295.575	0.4810069	-0.02	0.00	0.04	0.20
	2	1	0	2	0	2	2X5.455	0.4728200	-0.01	0.00	0.04	0.17
	2	1	0	2	0	1	2X5.465	0.4727871	-0.01	0.00	0.04	0.14

<sup>a</sup>The units are  $\mu\text{s}$ .  $\gamma$  denotes Greenwich Mean Sidereal Time +  $\pi$ . Values are based upon ocean tide angular momentum predictions at the eight primary diurnal and semidiurnal tidal frequencies from the TPX08 ocean tide model, followed by a smooth response assumption at other tidal frequencies. Digits X and E in Doodson numbers represent values of 10 and 11, respectively.

formed as linear combinations of the Fourier series terms given the spectrum of the tide-generating potential. As mentioned earlier, in the diurnal band we explicitly ignore the retrograde component of the predicted tidal variations in polar motion, following conventions that account for these effects in the nutation model.

As shown by *Desai and Wahr* [1995], the most important factor in choosing the ocean tide response functions is the number of parameters, namely, degrees of freedom, that are used to represent those functions rather than the functional form. We verified this is also true for the EOP response functions by comparing predicted EOP variations determined from our nominal Fourier series approach in equation (5) with an approach that uses quadratic functions in frequency instead. The amplitudes of resulting differences in the predicted EOPs are less than  $0.4 \mu\text{s}$  in each of the two polar motion parameters ( $p_1$  and  $p_2$ ) and less than  $0.4$  microseconds in LOD for all tidal frequencies with four exceptions. The amplitudes of the differences at the  $J_1$ ,  $OO_1$ ,  $OO_1$  nodal modulation, and  $v_1$  tidal frequencies are  $0.6$ ,  $1.0$ ,  $0.6$ , and  $0.4 \mu\text{s}$  in polar motion, and  $0.8$ ,  $1.3$ ,  $0.9$ ,

and  $0.6 \mu\text{s}$  in LOD. All of these cases have larger frequencies than the  $K_1$  tide. Larger errors in the response functions are expected at frequencies outside of the range spanned by the two bounding frequencies that are used to determine those functions. In our case, the bounding frequencies are  $Q_1$  and  $K_1$  in the diurnal band, and  $N_2$  and  $K_2$ , in the semidiurnal band. Within the range of those bounding frequencies the response functions are essentially interpolating functions, but outside of that range they are extrapolating functions and therefore prone to larger errors. These metrics provide some measure of the interpolation/extrapolation error induced by the response function approach. We note that the software provided with the TPX08 ocean tide model uses a piecewise-linear interpolation approach for the smooth admittance functions and is an alternative that may be worth considering for extrapolation of the admittances.

The application of the smooth response assumption to the ocean tide angular momentum, instead of the EOPs, would eliminate the need for the response functions to accommodate frequency dependent effects in the conversion to EOPs. For example, the conversion to polar motion in equation (2) is inversely proportional to the tidal frequency. However, this is mitigated by the fact that the smooth response functions are applied over a relatively narrow bandwidth at frequencies that are not close to the resonant frequencies of equation (2) (especially since we are ignoring retrograde diurnal polar motion variations). We have confirmed that applying the smooth response assumption to angular momentum functions instead of the EOPs results in polar motion predictions whose differences have amplitudes of less than  $0.1 \mu\text{s}$  at all except six diurnal frequencies, all of which are in the extrapolation region with frequencies larger than  $K_1$ . Even then, differences are less than  $0.6 \mu\text{s}$  at all frequencies. Differences larger than  $0.2 \mu\text{s}$  in LOD are also limited to those same six frequencies, peaking at  $1.1 \mu\text{s}$  for  $OO_1$ .

Tables A1 and A2 provide the resulting TPX08-based predicted diurnal and semidiurnal variations in polar motion and LOD for those tidal frequencies that have predicted amplitudes larger than  $0.1 \mu\text{s}$  in either  $p_1$  or  $p_2$ , or  $0.1 \mu\text{s}$  in LOD. Values with a precision of one order of magnitude smaller are intentionally used only to avoid roundoff at the cutoff levels. The predicted variations in LOD are computed using equation (6) from Gross [1993]. Both tables provide the same frequencies for the convenience of interconsistency. The phase conventions in Tables A1 and A2 follow that of Tables 8.2 and 8.3 in Petit and Luzum [2010], again for ease of comparison. With the specified thresholds, we provide 86 diurnal and 73 semidiurnal tidal components, compared to their provision of 41 and 30 respective components. Values from these two tables are also provided as supporting information to this paper in the form of an ASCII text file. For the four semidiurnal tidal components shown in Table 1 the phase conventions are the same as used in Tables A1 and A2. For the four diurnal tidal components, the Greenwich phase lags used in Table 1,  $\phi$ , are related to the phase lags of Tables A1 and A2, say  $\phi'$ , as follows  $\phi = \phi' - \pi/2$  for  $Q_1$ ,  $O_1$ , and  $P_1$ , and  $\phi = \phi' + \pi/2$  for  $K_1$ .

## Acknowledgments

S.D.D. and A.E.S. performed the work described in this paper at the Jet Propulsion Laboratory, California Institute of Technology under contract with the National Aeronautics and Space Administration. The authors thank G. Egbert and L. Erofeeva for making the TPX08 global models of the ocean tide height and mass transport publicly available at [http://volkov.oce.orst.edu/tides/tpxo8\\_atlas.html](http://volkov.oce.orst.edu/tides/tpxo8_atlas.html) and for feedback on an early draft of this paper. The authors also thank the Associate Editor, an anonymous reviewer, and Richard Ray for their reviews and feedback on this paper. The International GNSS Service and its member agencies are acknowledged for providing tracking data from globally distributed GNSS stations. Information on IGS data availability is provided at <http://igs.org>. The International Earth Rotation Service provided the EOPC04 daily time series of polar motion at <https://hpiers.obspm.fr/iers/eop/eopc04/>.

## References

- Altamimi, Z., X. Collilieux, and L. Métivier (2011), ITRF2008: An improved solution of the international terrestrial reference frame, *J. Geod.*, **85**(8), 457–473, doi:10.1007/s00190-011-0444-4.
- Artz, T., S. Tesmer née Böckmann, and A. Nothnagel (2011), Assessment of periodic sub-diurnal Earth rotation variations at tidal frequencies through transformation of VLBI normal equation systems, *J. Geod.*, **85**, 565–584, doi:10.1007/s00190-011-0457-z.
- Artz, T., L. Bernhard, A. Nothnagel, P. Steigenberger, and S. Tesmer (2012), Methodology for the combination of sub-daily Earth rotation from GPS and VLBI observations, *J. Geod.*, **86**(3), 221–239, doi:10.1007/s00190-011-0512-9.
- Brosche, P., U. Seiler, J. Sundermann, and J. Wunsch (1989), Periodic changes in Earth's rotation due to ocean tides, *Astron. Astrophys.*, **220**, 318–320.
- Brzeziński, A., and N. Capitaine (2002), Lunisolar perturbations in Earth rotation due to the triaxial figure of the Earth: Geophysical aspects, in *Proc. Journées Systèmes de Référence Spatio-Temporels 2001*, edited by N. Capitaine, pp. 51–58, Paris Observatory, Paris.
- Brzeziński, A., and P. M. Mathews (2003), Recent advances in modeling the lunisolar perturbations in polar motion corresponding to high frequency nutation: Report on the discussion of the IAU Commission 19 WG on Nutation, in *Proc. of the Journées 2002 – Systèmes de Référence Spatio-temporels*, edited by N. Capitaine and M. Stavinschi, pp. 101–108, Paris Observatory, Paris.
- Brzeziński, A., R. M. Ponte, and A. H. Ali (2004), Non-tidal oceanic excitation of nutation and diurnal/semidiurnal polar motion revisited, *J. Geophys. Res.*, **109**, B11407, doi:10.1029/2004JB003054.
- Cartwright, D. E., and R. D. Ray (1990), Oceanic tides from Geosat altimetry, *J. Geophys. Res.*, **95**(C3), 3069–3090, doi:10.1029/JC095iC03p03069.
- Chao, B. F., and R. D. Ray (1997), Oceanic tidal angular momentum and Earth's rotation variations, *Prog. Oceanogr.*, **40**, 399–421, doi:10.1016/S0079-6611(98)00010-X.
- Chao, B. F., D. N. Dong, H. S. Liu, and T. A. Herring (1991), Libration in the Earth's rotation, *Geophys. Res. Lett.*, **18**(11), 2007–2010, doi:10.1029/91GL02491.
- Chao, B. F., R. D. Ray, J. M. Gipson, G. D. Egbert, and C. Ma (1996), Diurnal/semidiurnal polar motion excited by oceanic tidal angular momentum, *J. Geophys. Res.*, **101**(B9), 20,151–20,163, doi:10.1029/96JB01649.
- Desai, S. D., and J. M. Wahr (1995), Empirical ocean tide models estimated from TOPEX/POSEIDON altimetry, *J. Geophys. Res.*, **100**(C12), 25,205–25,228, doi:10.1029/95JC02258.

- Egbert, G. D., and S. Y. Erofeeva (2002), Efficient inverse modeling of barotropic ocean tides, *J. Atmos. Oceanic Technol.*, *19*(2), 183–204, doi:10.1175/1520-0426.
- Egbert, G. D., A. F. Bennett, and M. G. G. Foreman (1994), TOPEX/Poseidon tides estimated using a global inverse model, *J. Geophys. Res.*, *99*, 24,821–24,852, doi:10.1029/94JC01894.
- Englich, S., P. J. Mendes-Cerveira, R. Weber, and H. Shuh (2007), Determination of Earth rotation variations by means of VLBI and GPS and comparison to conventional models, *Vermessung Geoinf.*, 104–112.
- Getino, J., J. M. Ferrándiz, and A. Escapa (2001), Hamiltonian theory for the non-rigid Earth: Semidiurnal terms, *Astron. Astrophys.*, *30*, 330–341, doi:10.1051/0004-6361:20010186.
- Gipson, J. M. (1996), Very long baseline interferometry determination of neglected tidal terms in high-frequency Earth orientation variation, *J. Geophys. Res.*, *101*(B12), 28,051–28,064, doi:10.1029/96JB02292.
- Gross, R. S. (1992), Correspondence between theory and observations of polar motion, *Geophys. J. Int.*, *109*, 162–170, doi:10.1111/j.1365-246X.1992.tb00086.x.
- Gross, R. S. (1993), The effect of ocean tides on the Earth's rotation as predicted by the results of an ocean tide model, *Geophys. Res. Lett.*, *20*(4), 293–296, doi:10.1029/93GL00297.
- Gross, R. S. (2015), Earth rotation variations—Long period, in *Geodesy, Treatise on Geophysics*, 2nd ed., vol. 3, Elsevier, Amsterdam, doi:10.1016/B978-0-444-53802-4.00059-2.
- Groves, G. W., and R. W. Reynolds (1975), An orthogonalized convolution method of tide prediction, *J. Geophys. Res.*, *80*(30), 4131–4138, doi:10.1029/JC080i030p04131.
- Herring, T. A., and D. Dong (1994), Measurement of diurnal and semidiurnal rotational variations and tidal parameters of Earth, *J. Geophys. Res.*, *99*(B9), 18,051–18,071, doi:10.1029/94JB00341.
- Kinoshita, H. (1977), Theory of the rotation of the rigid Earth, *Cel. Mech.*, *15*(3), 277–326, doi:10.1007/BF01228425.
- Mathews, P. M., and P. Bretagnon (2003), Polar motions equivalent to high frequency nutations for a non-rigid Earth with anelastic mantle, *Astron. Astrophys.*, *400*, 1113–1128, doi:10.1051/0004-6361.
- Mathews, P. M., T. A. Herring, and B. A. Buffet (2002), Modeling of nutation and precession: New nutation series for non-rigid Earth and insights into the Earth's interior, *J. Geophys. Res.*, *107*(B4), 2068, doi:10.1029/2001JB000390.
- Munk, W. H., and D. E. Cartwright (1966), Tidal spectroscopy and predictions, *Phil. Trans. R. Soc. London Ser. A*, *259*, 533–581, doi:10.1098/rsta.1966.0024.
- Munk, W. H., and G. J. F. Macdonald (1960), *The Rotation of the Earth, A Geophysical Discussion*, Cambridge Univ. Press, New York.
- Petit, G., and B. Luzum (2010), *IERS Conventions (2010)*, pp. 179, IERS Tech, Frankfurt, Germany. Note 36.
- Ray, R. D., and G. D. Egbert (2004), The global S1 tide, *J. Phys. Oceanogr.*, *34*, 1922–1935, doi:10.1175/1520-0485(2004)034<1922:TGST>2.0.CO;2.
- Ray, R. D., D. J. Steinberg, B. F. Chao, and D. E. Cartwright (1994), Diurnal and semidiurnal variations in the Earth's rotation rate induced by oceanic tides, *Science*, *264*(5160), 830–832, doi:10.1126/science.264.5160.830.
- Ray, R. D., B. F. Chao, Z. Kowalik, and A. Y. Proshutiksky (1996), Angular momentum of Arctic Ocean tides, *J. Geod.*, *71*, 344–350, doi:10.1007/s001900050102.
- Rothacher, M., G. Beutler, R. Weber, and J. Hefty (2001), High-frequency variations in Earth rotation from Global Positioning System data, *J. Geophys. Res.*, *106*(B7), 13,711–13,738, doi:10.1029/2000JB900393.
- Sasao, T., and J. M. Wahr (1981), An excitation mechanism for the free 'core nutation', *Geophys. J. Int.*, *64*(3), 729–746, doi:10.1111/j.1365-246X.1981.tb02692.x.
- Seiler, U. (1991), Periodic changes of the angular momentum budget due to the tides of the World Ocean, *J. Geophys. Res.*, *96*(B6), 10,287–10,300, doi:10.1029/91JB00219.
- Sibois, A. (2011), GPS-based estimation of polar motion parameters at sub-hourly frequency: Strategies and applications, PhD thesis, Univ. of Colo., Boulder.
- Stammer, D., et al. (2014), Accuracy assessment of global barotropic ocean tide models, *Rev. Geophys.*, *52*, 243–282, doi:10.1002/2014RG000450.
- Watkins, M. M., and R. J. Eanes (1994), Diurnal and semidiurnal variations in Earth orientation determined from LAGEOS laser ranging, *J. Geophys. Res.*, *99*(B9), 18,073–18,079, doi:10.1029/94JB00805.
- Wilson, C. R., and R. O. Vicente (1980), An analysis of the homogeneous ILS polar motion series, *Geophys. J. Int.*, *62*(3), 605–616, doi:10.1111/j.1365-246X.1980.tb02594.x.